Supporting Information

Caged Bulky Organic Dyes in a Polyaromatic Framework and Their Spectroscopic Peculiarities

Mayuko Ueda, Natsuki Kishida, Lorenzo Catti, and Michito Yoshizawa*

Laboratory for Chemistry and Life Science, Institute of Innovative Research, Tokyo Institute of Technology, 4259 Nagatsuta, Midori-ku, Yokohama 226-8503, Japan

Contents

Materials and methods

NMR: Bruker AVANCE HD400 (400 MHz) and HD500 (500 MHz), MALDI-TOF MS: Bruker ultrafleXtreme, ESI-TOF MS: Bruker micrOTOF II, UV-vis: JASCO V-670DS, Fluorescence: Hitachi F-7000, Absolute PL quantum yield: Hamamatsu C9920-02G with an integration sphere, FT-IR: SHIMADZU IRSpirit-T, Fluorescence lifetime: Hamamatsu C7700-ABS-N, DLS: Wyatt Technology DynaPro NanoStar, Molecular Modeling: BIOVIA Materials Studio 2020, version 20.1.0.5 (Dassault Systèmes Co.), DFT calculation: Gaussian 16 program package.

Solvents and reagents: TCI Co., Ltd., FUJIFILM Wako Chemical Co., Kanto Chemical Co., Inc., Sigma-Aldrich Co., and Cambridge Isotope Laboratories, Inc. Compounds: Compounds $\mathbf{7}_{n\mathrm{Br}}$ and **4b** were synthesized according to ref. S1 and S3, respectively.

References

[S1] M. Yamashina, T. Yuki, Y. Sei, M. Akita, M. Yoshizawa, *Chem. Eur. J.* **2015**, *21*, 4200–4204.

[S2] N. Kishi, Z. Li, K. Yoza, M. Akita, M. Yoshizawa, *J. Am. Chem. Soc.* **2011**, *133*, 11438–11441.

[S3] S. Jiang, J. Gao, L. Han, *Res. Chem. Intermed.* **2016**, *42*, 1017–1028.

[S4] C. L. D. Gibb, B. C. Gibb, *J. Am. Chem. Soc.* **2004**, *126*, 11408–11409.

Synthesis of compound 9 MU069, 071, 082

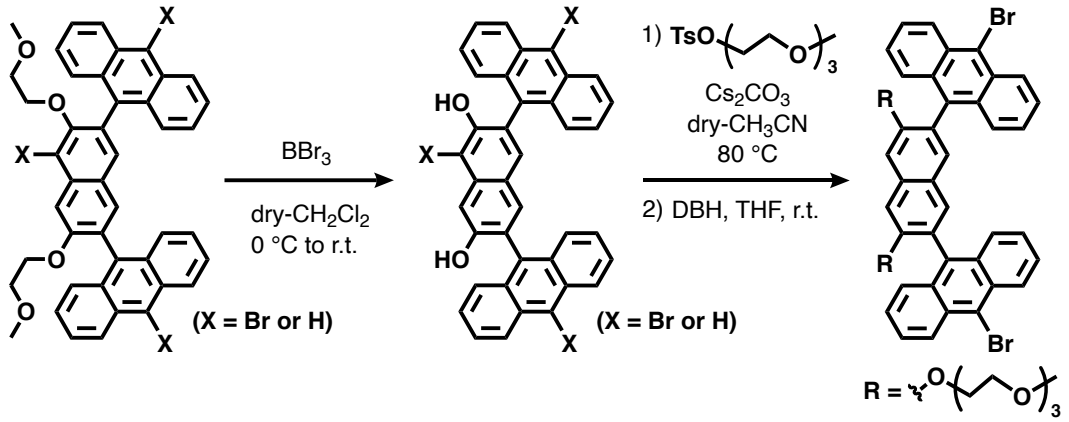

Compound $\mathbf{7}_{n\mathbf{Br}}$ (n = 1-3; 4.00 g, 5.09 mmol based on $\mathbf{7}_{\mathbf{2Br}}$) and dry CH_2Cl_2 (300 mL) were added to a 500 mL glass flask filled with N_2. A CH_2Cl_2 solution (1.0 M) of BBr_3 (20 mL, 20 mmol) was slowly added to the solution at 0 ºC and then the mixture was stirred at r.t. overnight. When water was added to the solution, yellow precipitate $\mathbf{8}_{n\mathbf{Br}}$ (n = 1-3; 4.28 g) was collected and dried under vacuum. Compound $\mathbf{8}_{n\mathbf{Br}}$ (n = 1-3; 4.00 g) and Cs_2CO_3 (11.8 g, 36.2 mmol) were added to a 500 mL glass flask filled with N_2. Dry CH_3CN (160 mL) was added to the flask and then the mixture was stirred at 85 ºC for 30 min. After addition of 2-(2-(2-methoxyethoxy)ethoxy)ethyl *p*-toluenesulfonate (5.46 g, 17.1 mmol), the mixture was stirred at 85 ºC overnight. The resultant solution was concentrated under reduced pressure. The crude product, 1,3-dibromo-5,5-dimethylhydantoin (DBH; 0.117 g, 0.407 mmol), and THF (70 mL) were added to a 200 mL glass flask at 0 ºC. The mixture was stirred at r.t. for 2 d. The resultant solution was concentrated under reduced pressure. The crude product was purified by silica gel column chromatography (EtOAc) to afford compound **9** as a yellow solid (0.628 g, 0.652 mmol, 14% based on $\mathbf{7}_{\mathbf{2Br}}$ (3 steps)).

Compound $\mathbf{8}_{n\mathbf{Br}}$: ^{1}H NMR (400 MHz, DMSO-d_6, r.t.): δ 9.78(s, 2H), 8.52 (d, J = 8.7 Hz, 4H), 7.78-7.68 (m, 10H), 7.52 (dd, J = 8.7, 6.6 Hz, 4H), 7.37 (s, 2H). MALDI-TOF MS (dithranol): m/z Calcd. for $C_{38}H_{22}Br_2O_2$ [$\mathbf{8}_{\mathbf{2Br}}$ – H]$^-$ 669.13, Found 668.99.

Compound **9**: ^{1}H NMR (400 MHz, $CDCl_3$, r.t.): δ 8.60 (d, J = 8.8 Hz, 4H), 7.73 (d, J = 8.6 Hz, 4H), 7.69 (s, 2H), 7.59 (ddd, J = 8.6, 6.6, 1.1 Hz, 4H), 7.44 (s, 2H), 7.39 (ddd, J = 8.8, 6.6, 1.1 Hz, 4H), 4.17 (t, J = 4.7 Hz, 4H), 3.45-3.38 (m, 8H), 3.36-3.33 (m, 4H), 3.32 (s, 6H), 2.99-2.95 (m, 4H), 2.85-2.81 (m, 4H). ^{13}C NMR (125 MHz, $CDCl_3$, r.t.): δ 156.5 (C_q), 134.3 (C_q), 131.8 (CH), 131.5 (C_q), 130.2 (C_q), 127.8 (CH), 127.4 (CH), 126.9 (CH), 125.5 (CH), 122.7 (C_q), 105.8 (CH), 71.7 (CH_2), 70.3 (CH_2), 70.2 (CH_2), 70.1 (CH_2),

68.9 (CH_2), 68.8 (CH_2), 58.9 (CH_3). FT-IR (ATR, cm^{-1}): 3073, 2915, 2872, 1629, 1433, 1245, 1218, 1104, 920, 874, 752. HR MS (ESI, CH_3CN): *m/z* Calcd. for $C_{52}H_{50}Br_2O_8Na$ [**9** + Na]$^+$ 985.1751, Found 985.1751.

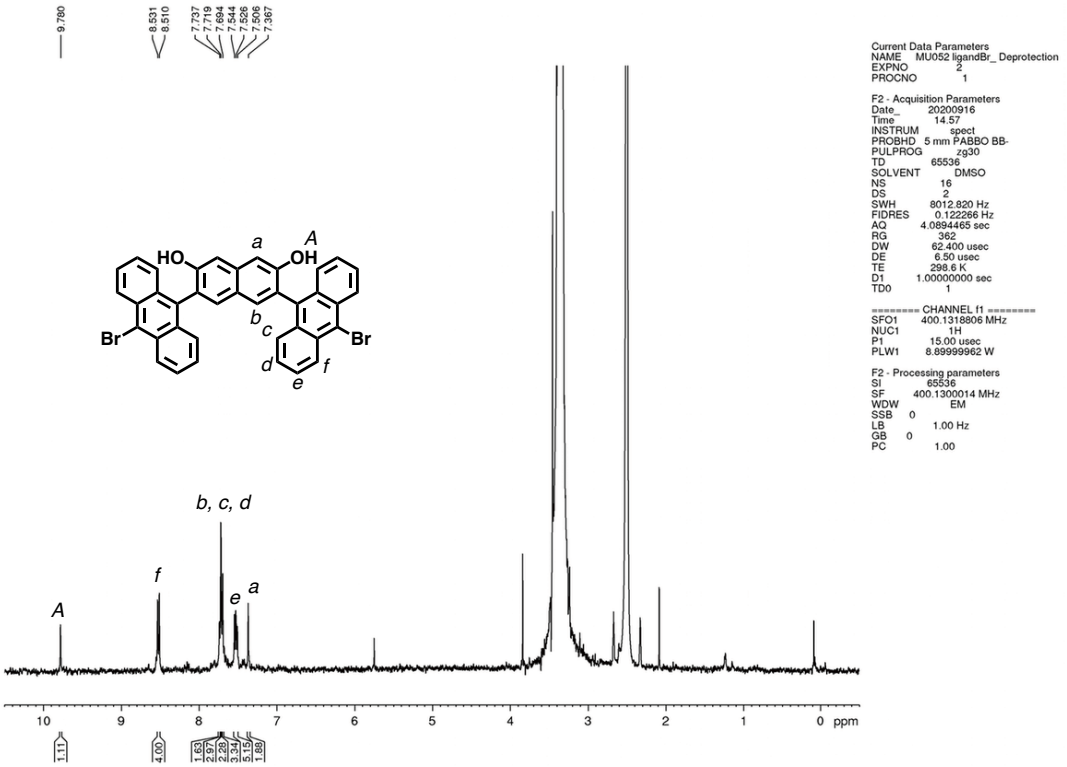

Figure S1. ^{1}H NMR spectrum (400 MHz, DMSO-d_6, r.t.) of $\mathbf{8}_{n\mathbf{Br}}$.

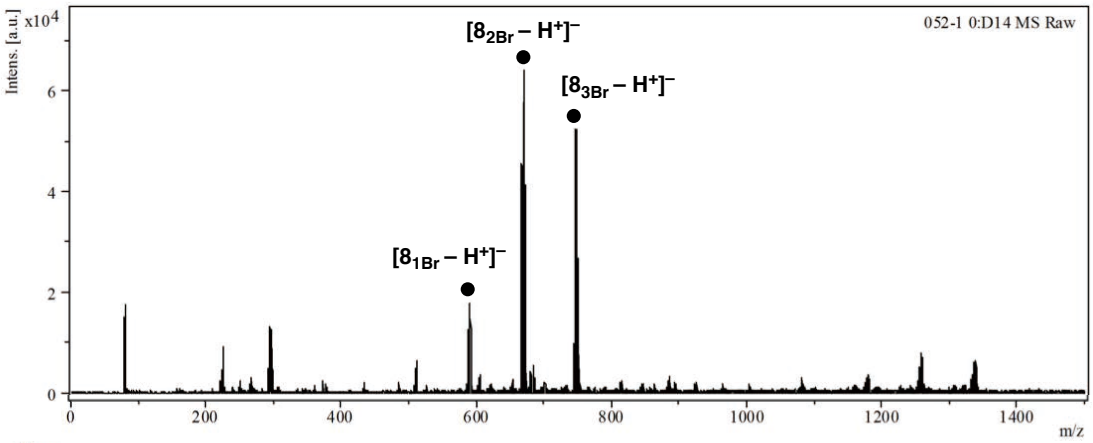

Acquisition Parameter

Date of acquisition	2020-09-17T11:17:45.233+09:00
Acquisition method name	D:\Methods\flexControlMethods\kinbara_lab\RN_0-3kDa.par
Aquisition operation mode	Reflector
Voltage polarity	NEG
Number of shots	1500
Name of spectrum used for calibration	
Calibration reference list used	NegPeptideCalibStandard mono

Instrument Info

User	testuser
Instrument	FLEX-PC
Instrument type	ultraflexTOF/TOF

Figure S2. MALDI-TOF MS spectrum (dithranol) of $\mathbf{8}_{n\mathbf{Br}}$.

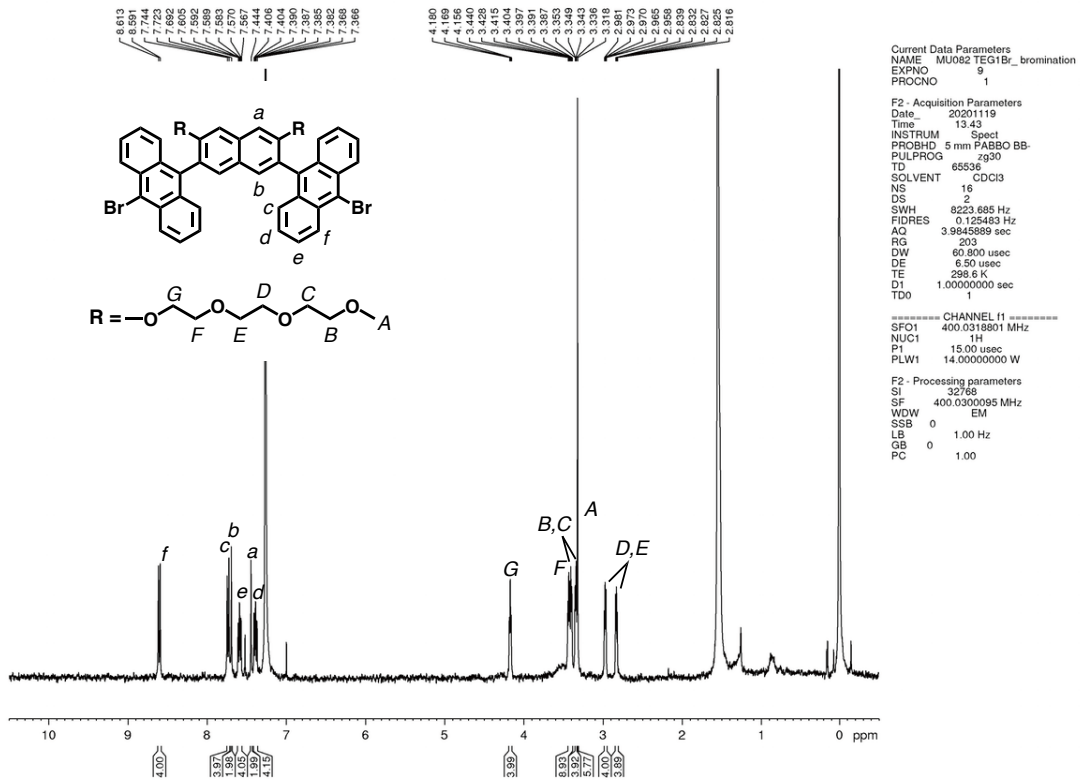

Figure S3. ^{1}H NMR spectrum (400 MHz, $CDCl_3$, r.t.) of **9**.

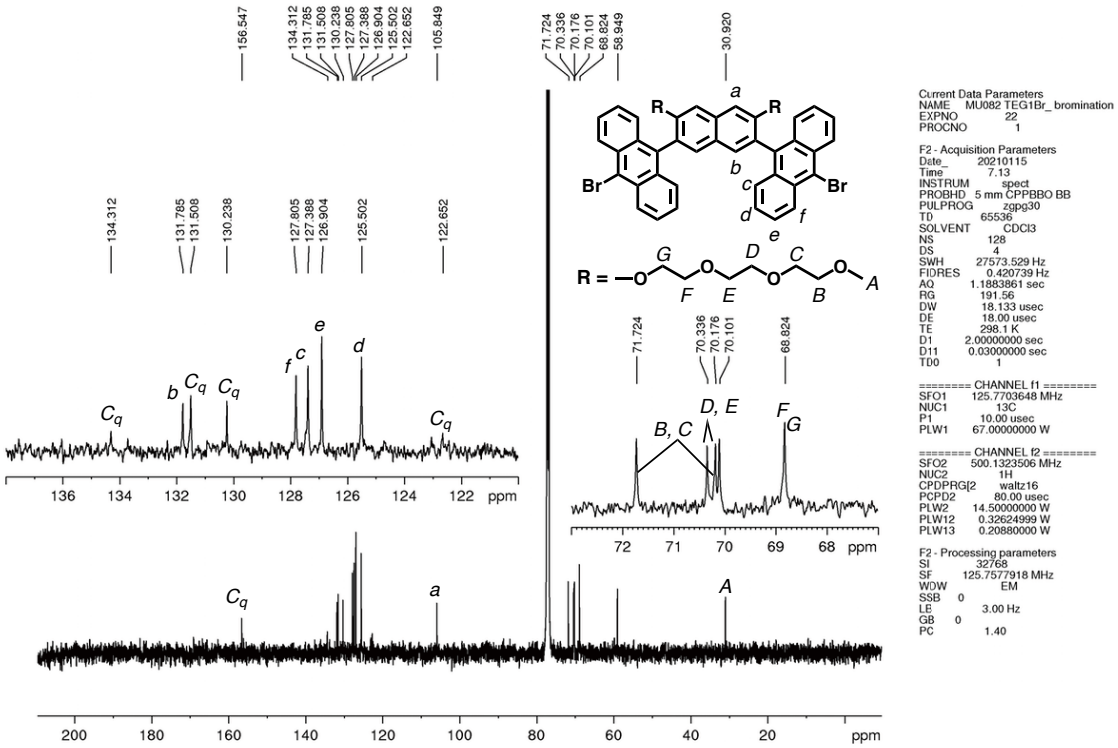

Figure S4. ^{13}C NMR spectrum (125 MHz, $CDCl_3$ r.t.) of **9**.

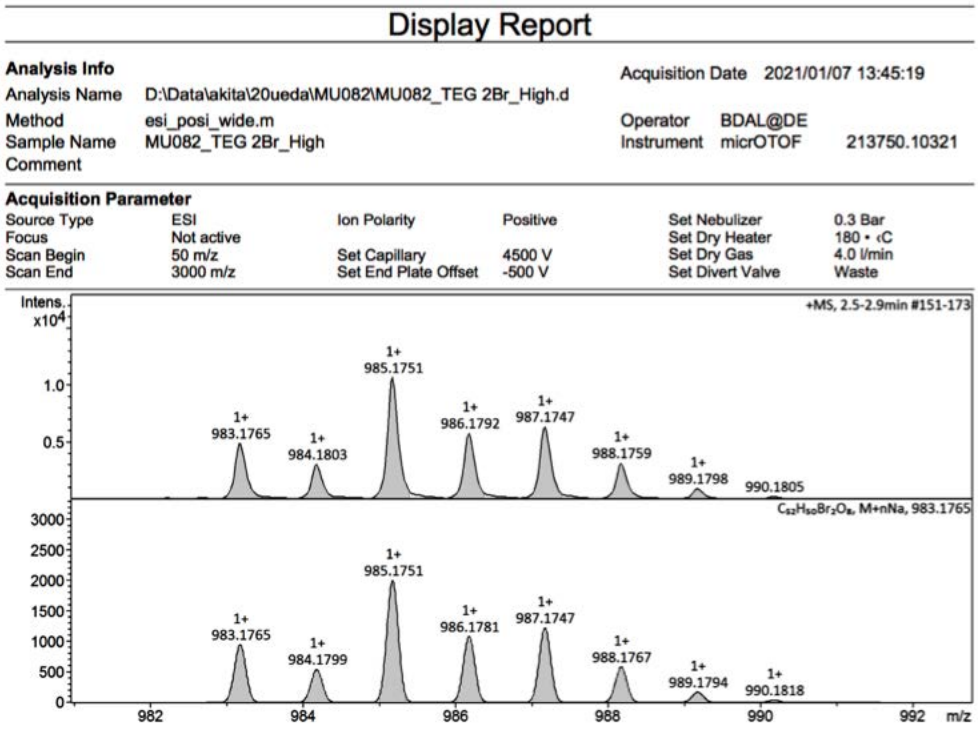

Figure S5. HR MS spectrum (ESI, CH_3CN) of **9**.

Synthesis of ligand 3 MU087

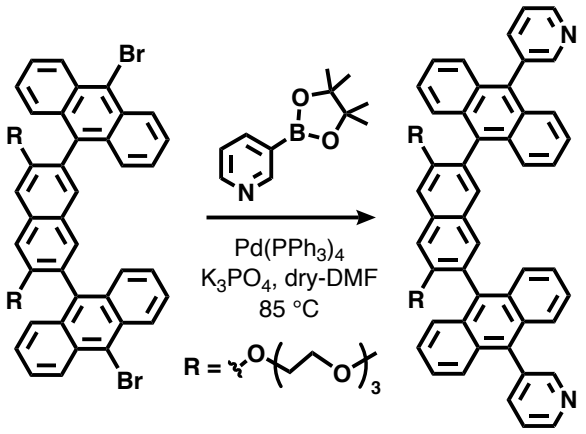

Compound **9** (0.60 g, 0.62 mmol), 3-pyridylboronic acid pinacol ester (0.38 g, 1.9 mmol), K_3PO_4 (0.80 g, 3.8 mmol), and $Pd(PPh_3)_4$ (0.078 g, 0.067 mmol) were added to a 200 mL glass flask filled with N_2. Dry and degassed DMF (60 mL) was added to the flask and then the mixture was stirred at 85 ºC for 17 h.[S2] The resultant solution was concentrated under reduced pressure. The crude product was purified by gel permeation chromatography ($CHCl_3$) to afford ligand **3** as a yellow solid (84.0 mg, 87.6 μmol, 14%). ^{1}H NMR (500 MHz, $CDCl_3$, r.t.): δ 8.83 (d, J = 4.8 Hz, 2H), 8.77 (s, 1H), 8.75 (s, 1H), 7.90-7.76 (m, 8H), 7.65-7.55 (m, 6H), 7.53-7.50 (m, 2H), 7.40-7.35 (m, 8H), 4.26-4.22 (br, 4H), 3.54-3.49 (m, 4H), 7.44-7.36 (m, 8H), 3.32 (s, 6H), 3.10-3.02 (m, 4H), 2.96-2.89 (m, 4H). ^{13}C NMR (125 MHz, $CDCl_3$, r.t.): δ 148.9-148.8 (C_q), 151.9-151.7 (CH), 148.9-148.8 (CH), 139.0-138.9 (CH), 136.0-135.9 (C_q), 135.0-134.9 (C_q), 134.7-134.6 (C_q), 132.6-132.5 (C_q), 132.0-131.8 (CH), 127.3-127.2 (CH), 126.2-126.1 (CH), 125.6-125.5 (CH), 125.1-125.0 (CH), 124.2-124.1 (C_q), 123.5-123.3 (CH), 106.0-105.8 (CH), 71.8-71.7 (CH_2), 70.5-70.4 (CH_2), 70.4-70.3 (CH_2), 70.2-70.1 (CH_2), 69.0-68.9 (CH_2), 68.9-68.7 (CH_2), 59.0-58.9 (CH_3). FT-IR (ATR, cm^{-1}): 3062, 2916, 2865, 1627, 1432, 1406, 1365, 1217, 1157, 1130, 1101, 1025, 766, 719. HR MS (ESI, CH_3CN): *m/z* Calcd. for $C_{62}H_{58}N_2O_8Na$ [**3** + Na]$^+$ 981.4104, Found 981.4085.

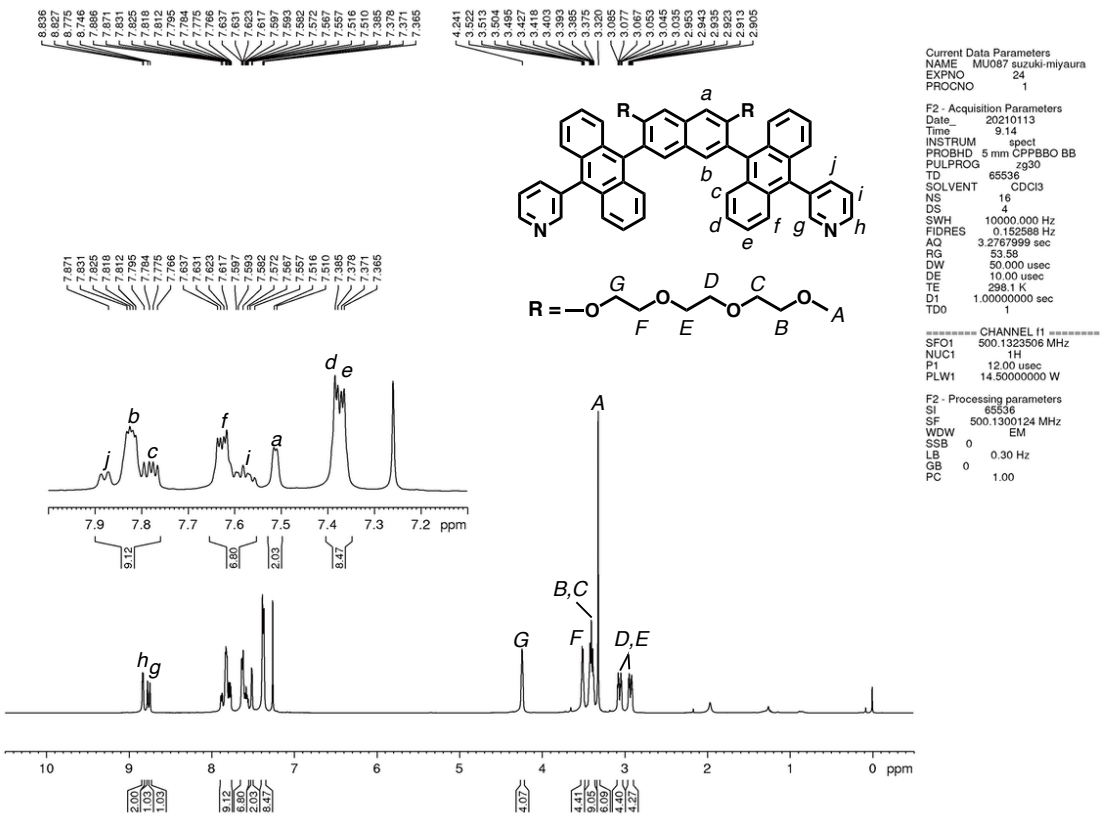

Figure S6. [1]H NMR spectrum (500 MHz, $CDCl_3$, r.t.) of **3**.

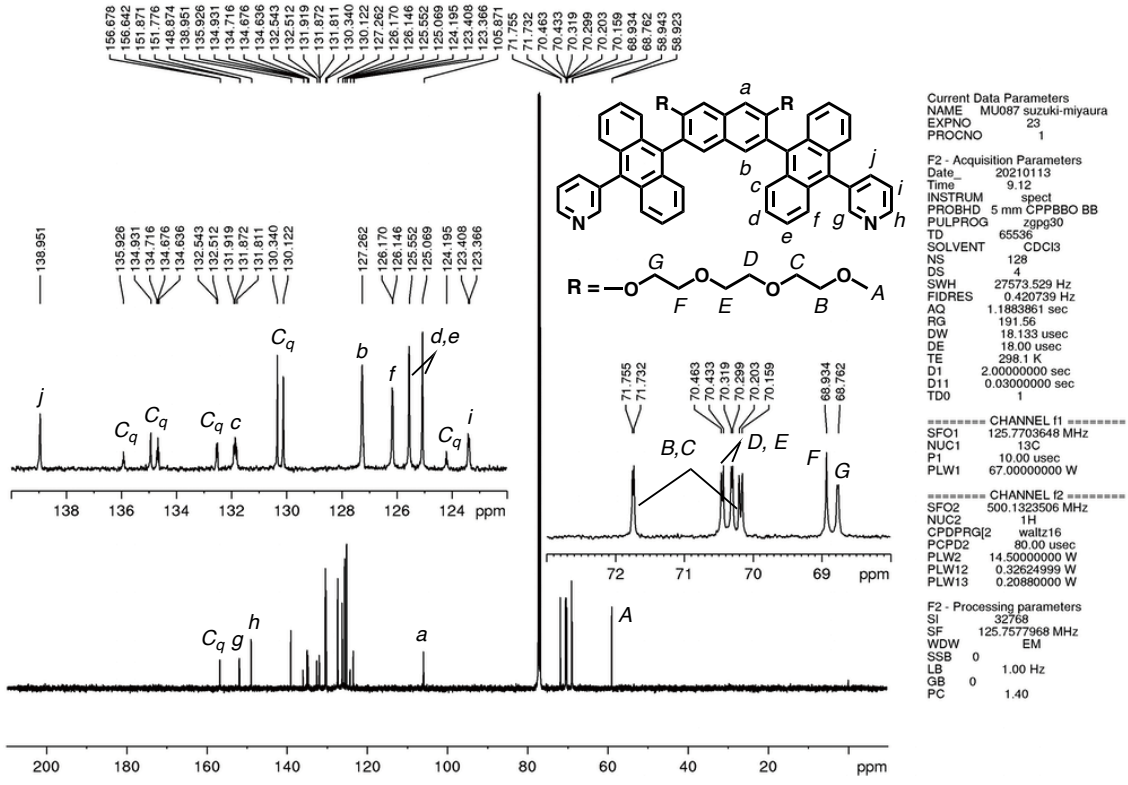

Figure S7. [13]C NMR spectrum (125 MHz, $CDCl_3$ r.t.) of **3**.

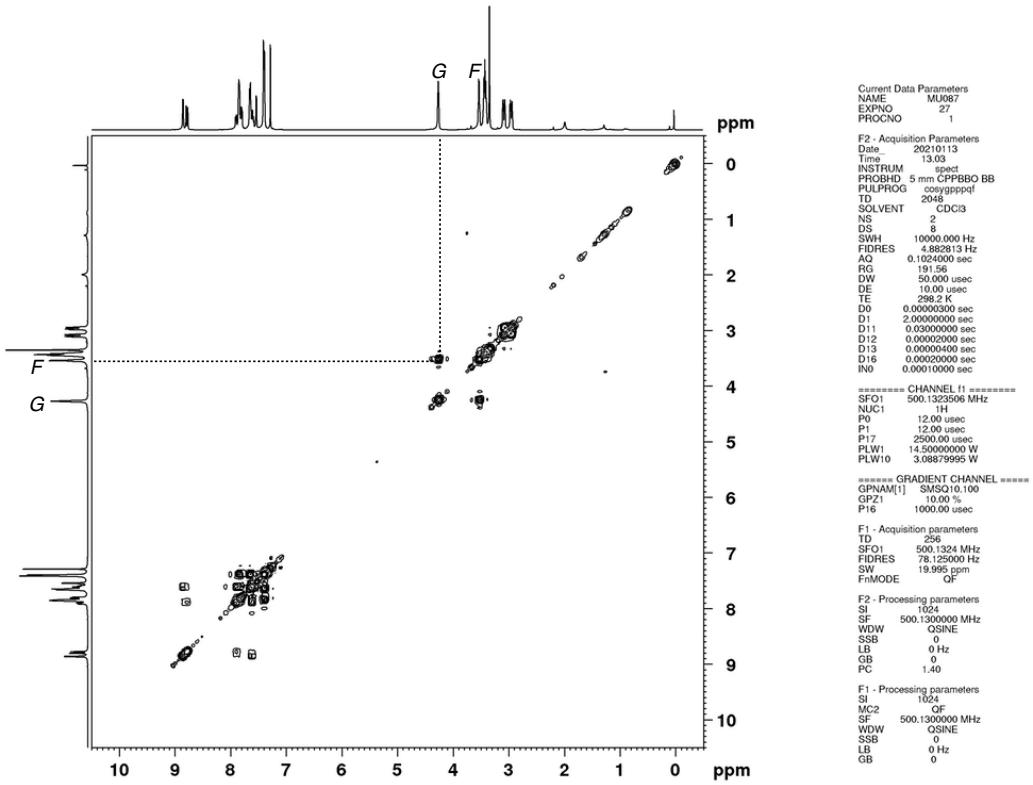

Figure S8a. ^{1}H-^{1}H COSY spectrum (500 MHz, $CDCl_3$, r.t.) of **3**.

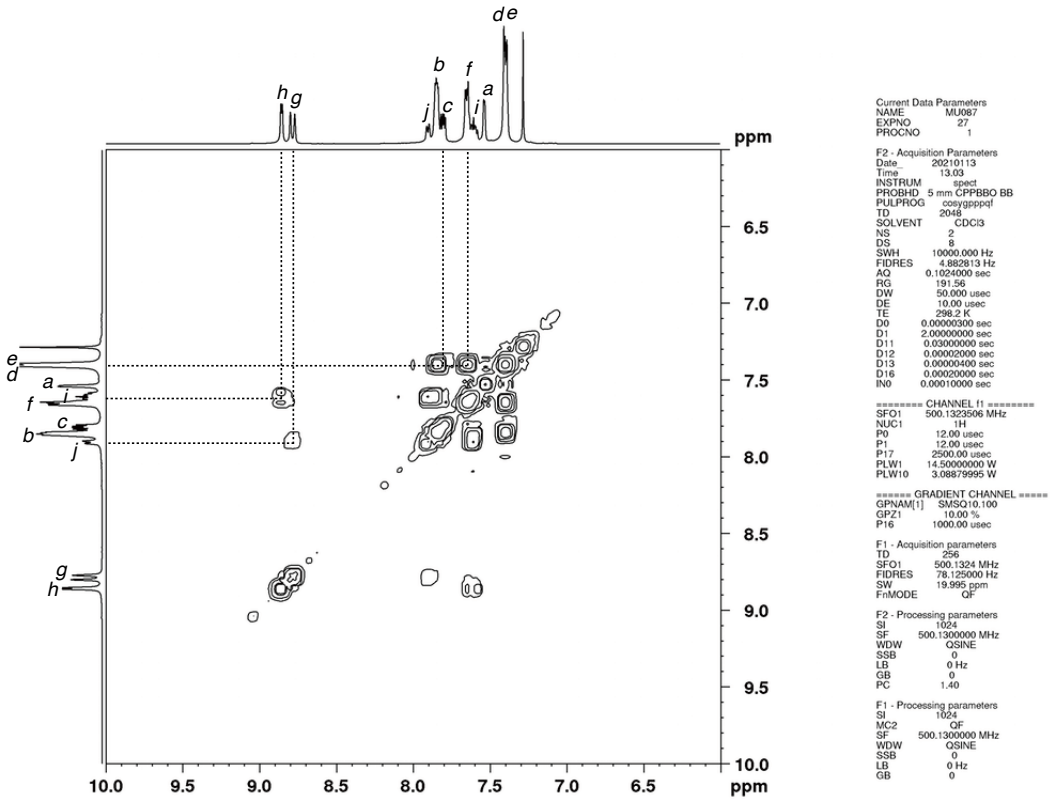

Figure S8b. ^{1}H-^{1}H COSY spectrum (500 MHz, $CDCl_3$, r.t.) of **3**.

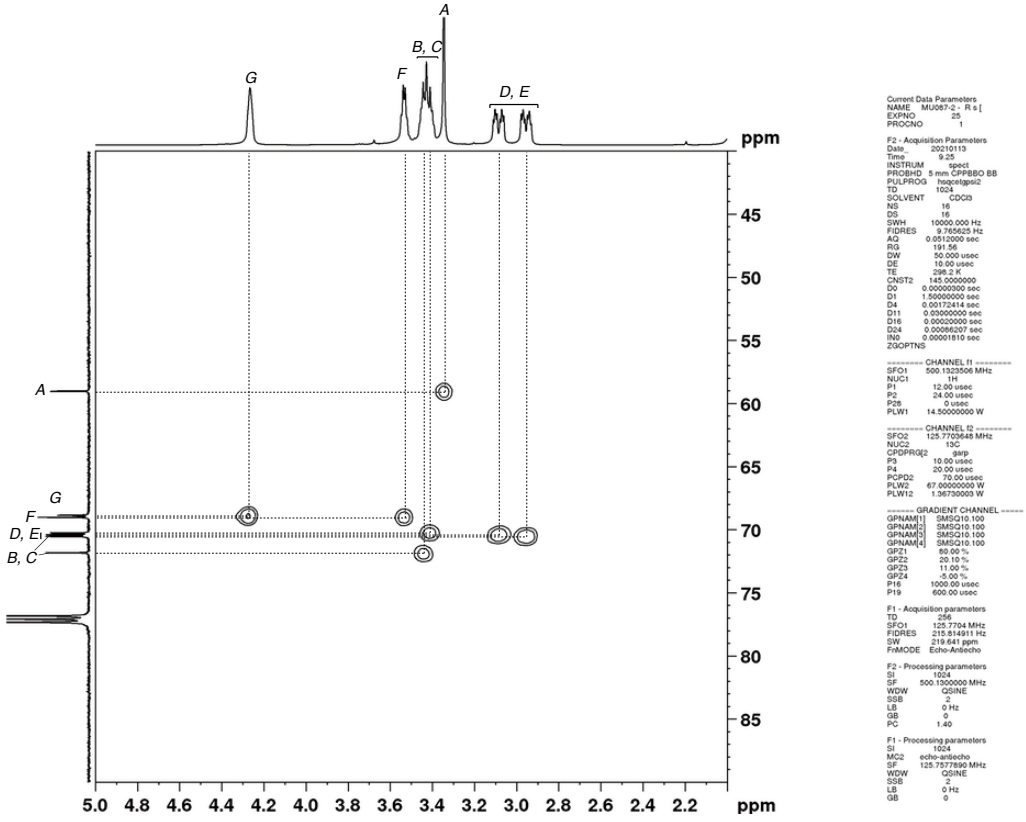

Figure S9a. HSQC spectrum (500 MHz, $CDCl_3$, r.t.) of **3**.

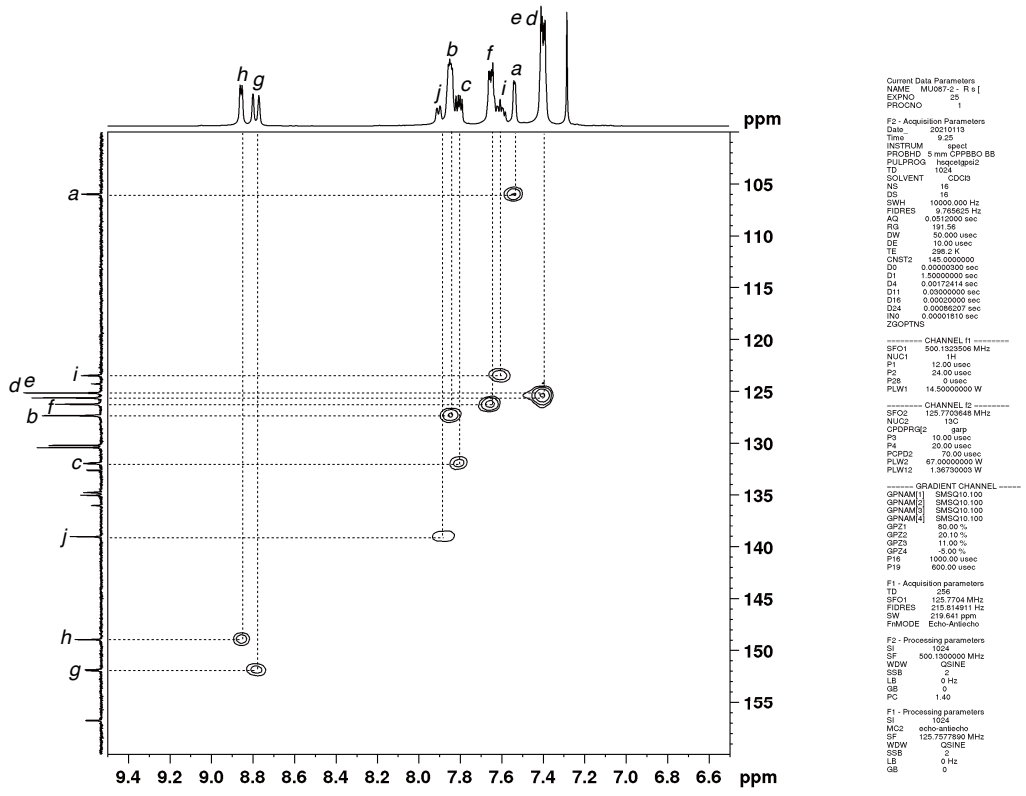

Figure S9b. HSQC spectrum (500 MHz, $CDCl_3$, r.t.) of **3**.

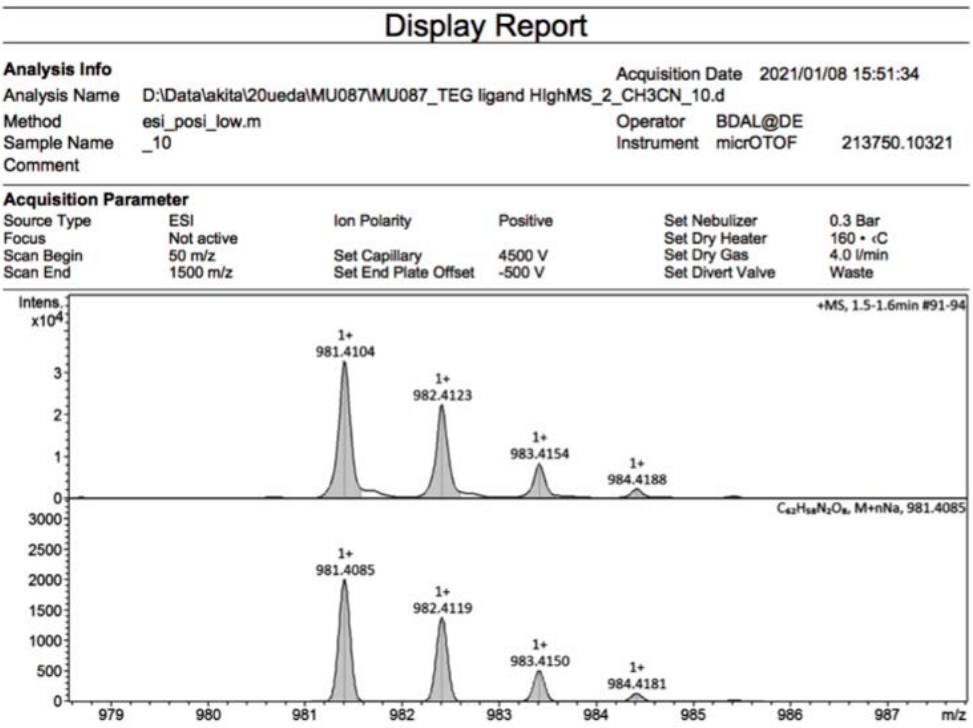

Figure S10. HR MS spectrum (ESI, CH_3CN) of **3**.

Formation of cage 1 MU348

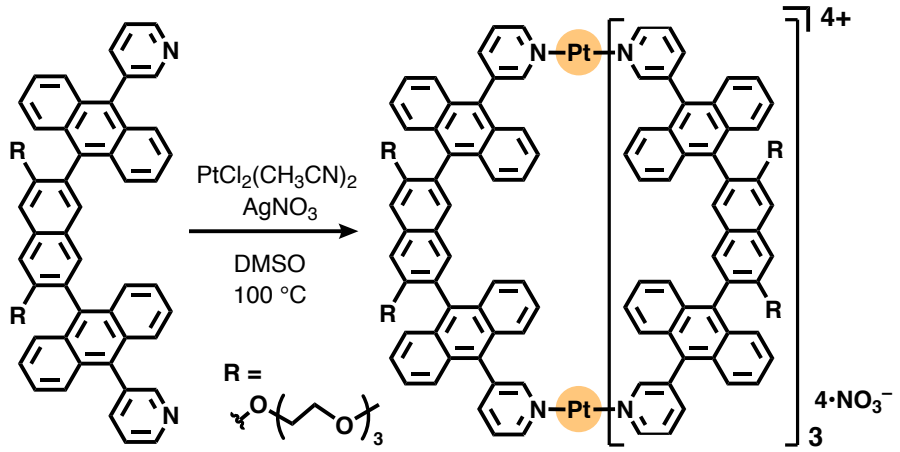

Ligand **3** (20.0 mg, 20.9 μmol), $PtCl_2(CH_3CN)_2$ (4.0 mg, 12 μmol), $AgNO_3$ (4.4 mg, 26 μmol), and DMSO-d_6 (0.5 mL) were added to a glass test tube and then the mixture was stirred at 100 ºC for 2 d to give cage **1** in a quantitative fashion. After evaporation of the solvent, the crude product was dissolved in CH_2Cl_2 and filtered through a membrane filter (pore size: 200 nm). When the resultant solution was reprecipitated with hexane, cage **1** was obtained as a yellow solid (20.6 mg, 4.6 μmol, 88% isolated yield).

^{1}H NMR (500 MHz, CD_3CN, r.t.): δ 9.33 (d, J = 5.6Hz, 8H), 8.44-8.39 (m, 16H), 8.22 (dd, J = 7.6, 5.6 Hz, 8H), 7.66 (s, 8H), 7.60 (d, J = 8.9 Hz, 16H), 7.26 (dd, J = 8.9, 7.2

Hz, 16H), 7.18 (s, 8H), 7.02 (dd, J = 8.9, 7.2 Hz, 16H), 6.77 (d, J = 8.9 Hz, 8H), 4.26-4.23 (m, 16H), 3.47-3.44 (m, 16H), 3.30-3.25 (m, 32H), 3.21 (s, 24H), 3.06-3.05 (br, 32H). ^{13}C NMR (125 MHz, CD_3CN, r.t.): δ 155.5 (C_q), 153.7 (CH), 151.5(CH), 143.3 (CH), 137.5 (C_q), 135.3 (C_q), 135.2 (C_q), 131.3 (CH), 128.8 (C_q), 128.6 (C_q), 127.7 (C_q), 127.0 (CH), 126.3 (CH), 125.7 (CH or C_q), 125.5 (CH or C_q), 124.5 (CH), 123.8 (CH), 123.1 (C_q), 105.5 (CH), 70.6 (CH_2), 69.2 (CH_2), 68.9 (CH_2), 68.9 (CH_2), 67.9 (CH_2), 67.6 (CH_2), 57.0 (CH_3). DOSY NMR (500 MHz, CD_3CN, 25 ºC): $D = 4.68 \times 10^{-10}$ m^2 s^{-1}. FT-IR (ATR, cm^{-1}): 3062, 2902, 2870, 2824, 1628, 1427, 1339, 1219, 1104, 1028, 769, 702. ESI-TOF MS (CH_3CN): m/z 1056.5 [**1** – 4•NO_3^-]$^{4+}$, 1429.4 [**1** – 3•NO_3^-]$^{3+}$, 2175.0 [**1** – 2•NO_3^-]$^{2+}$.

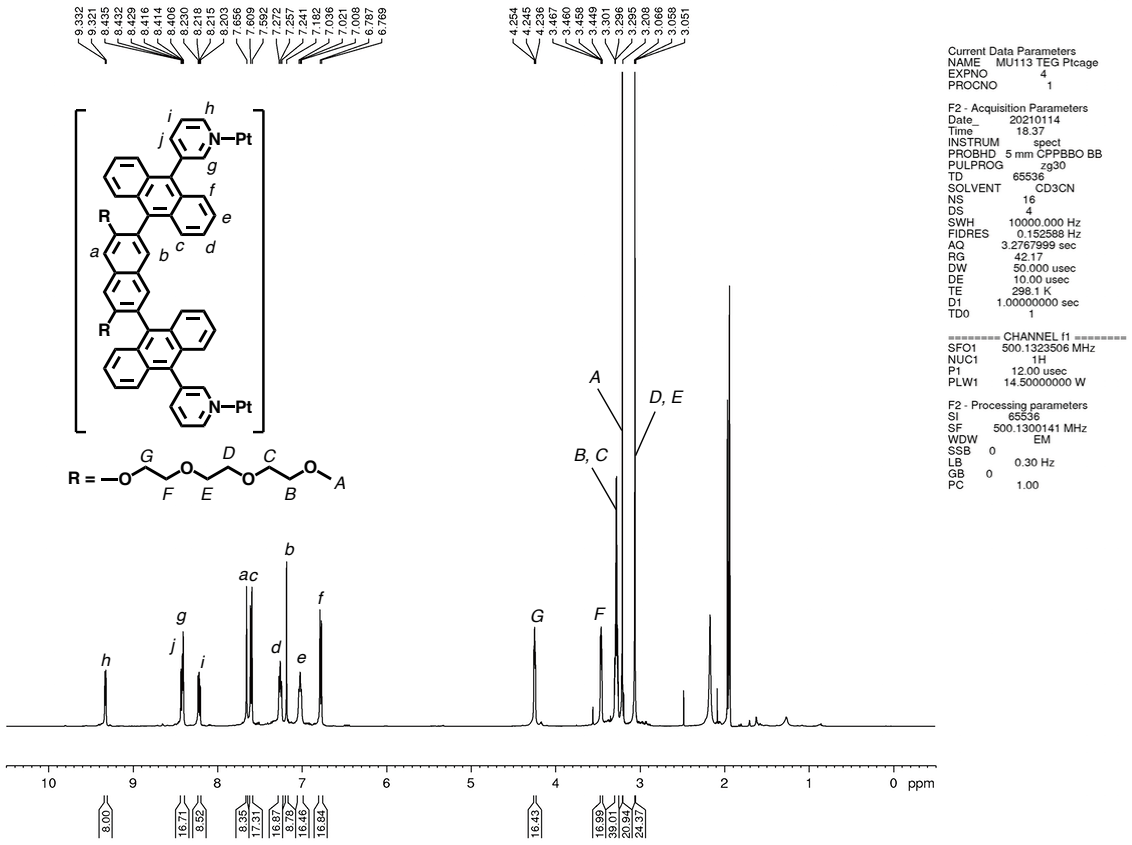

Figure S11. ^{1}H NMR spectrum (500 MHz, CD_3CN, r.t.) of **1**.

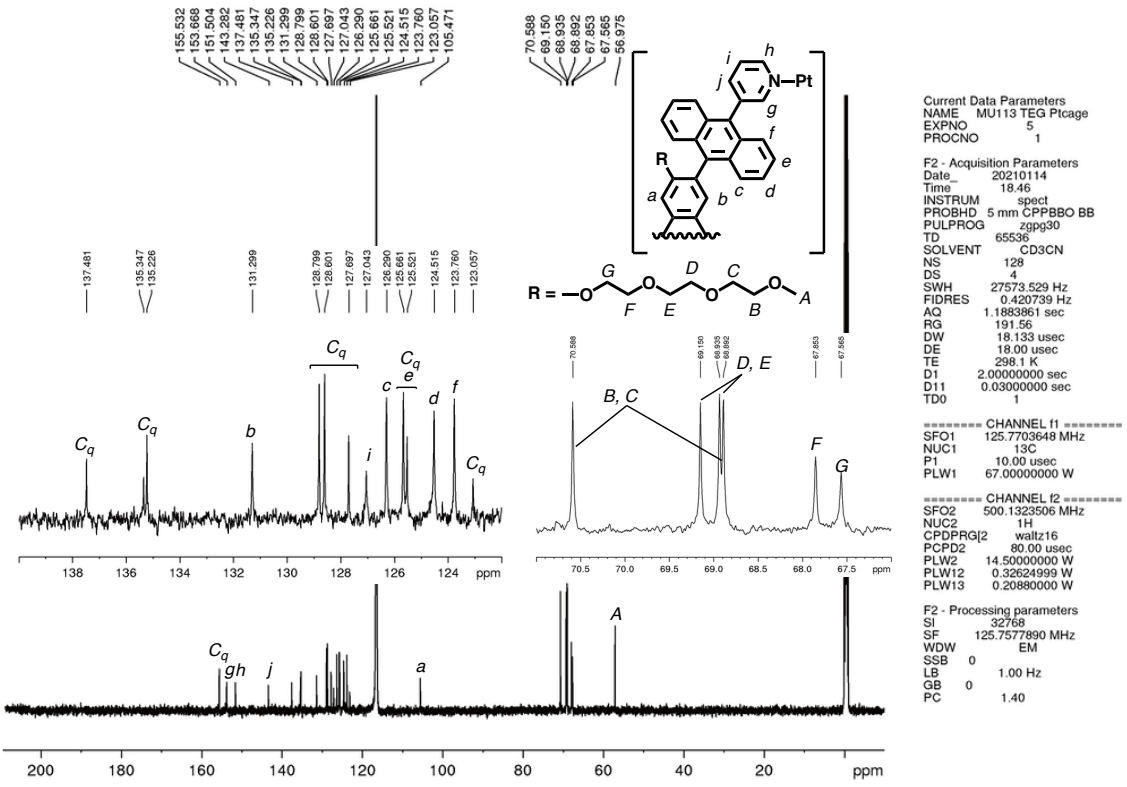

Figure S12. ^{13}C NMR spectrum (125 MHz, CD_3CN, r.t.) of **1**.

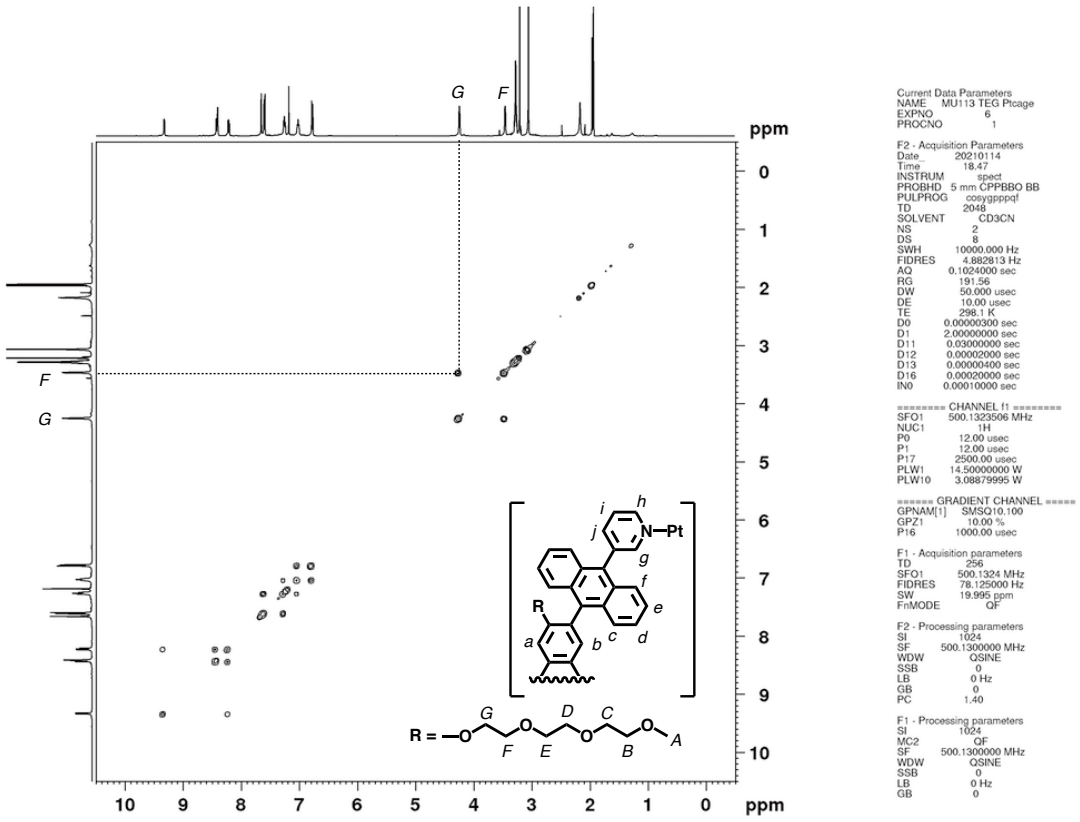

Figure S13a. ^{1}H-^{1}H COSY spectrum (500 MHz, CD_3CN, r.t.) of **1**.

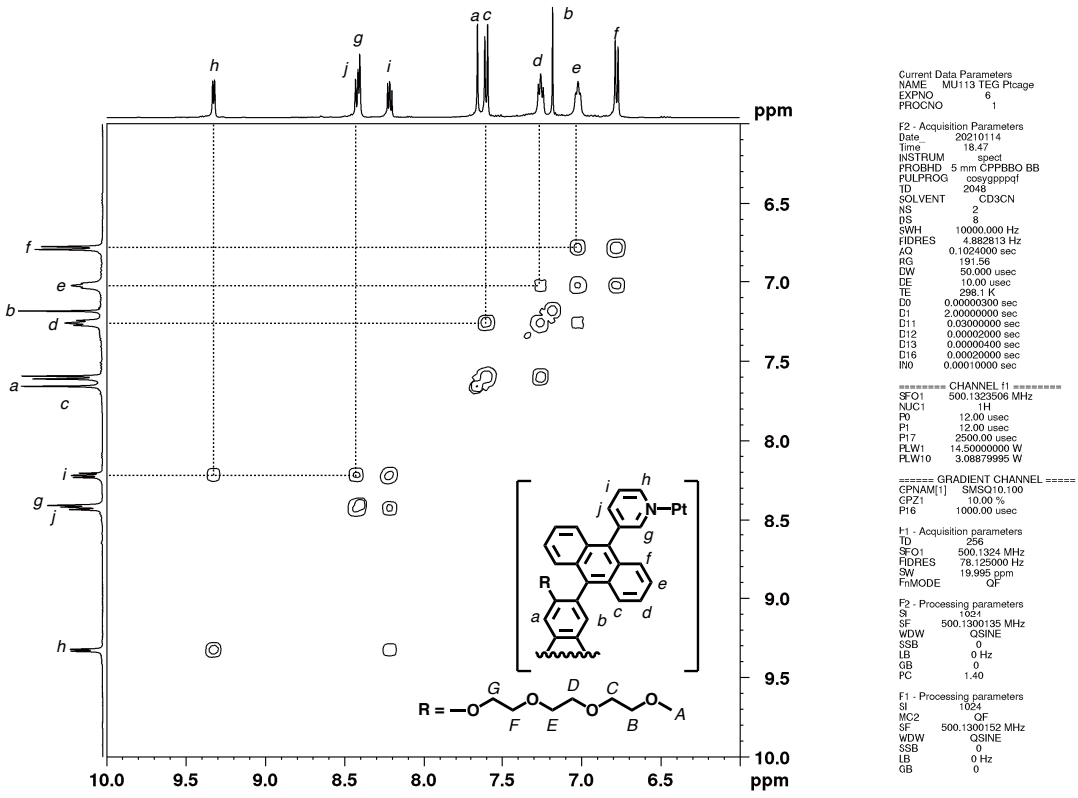

Figure S13b. ^{1}H-^{1}H COSY spectrum (500 MHz, CD_3CN, r.t.) of **1**.

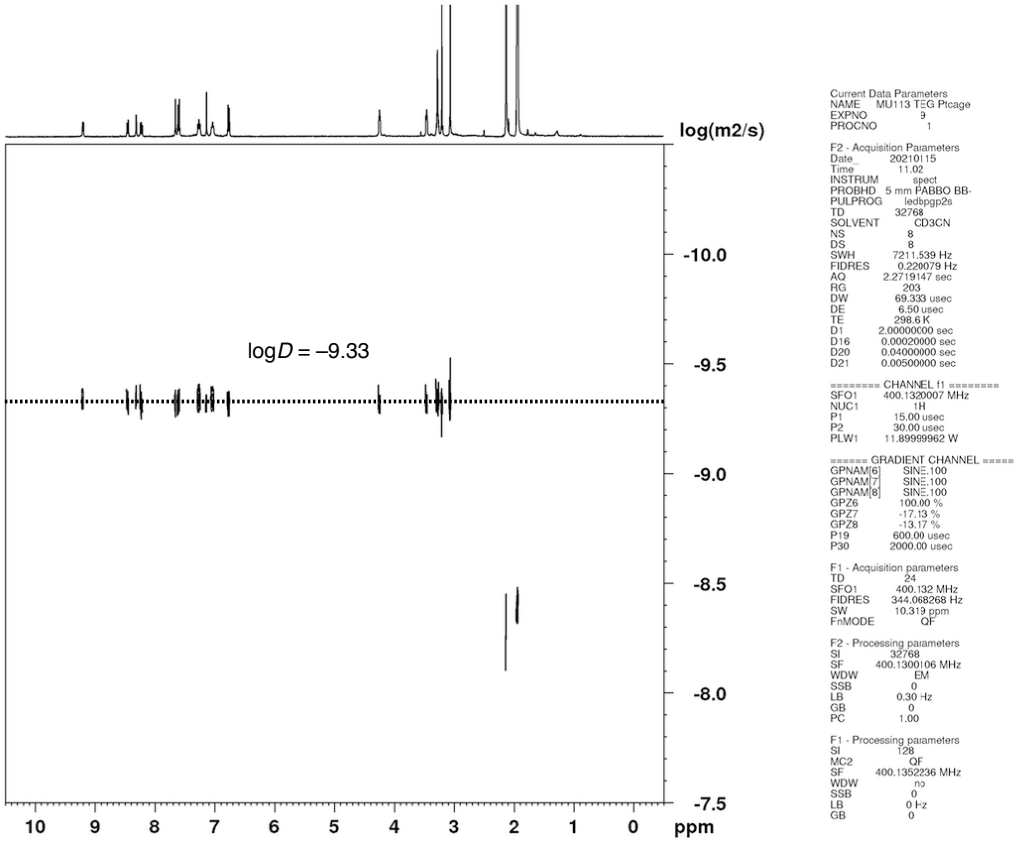

Figure S14. ^{1}H DOSY NMR (500 MHz, CD_3CN, 25 ºC) of **1**.

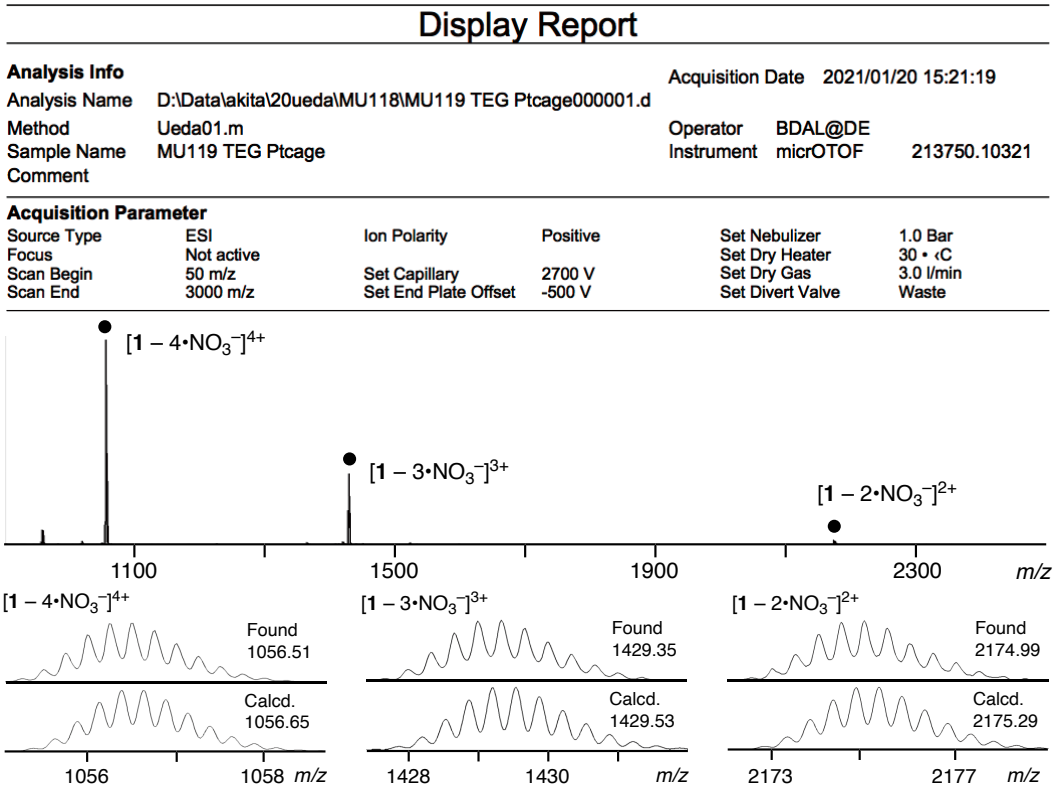

Figure S15. ESI-TOF MS spectrum (CD_3CN) of **1**.

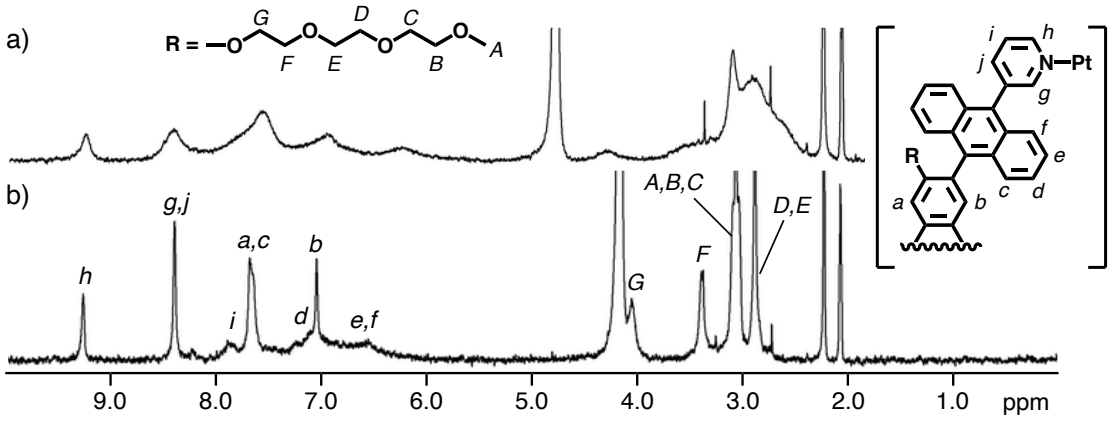

Figure S16. Temperature-dependent ^1H NMR spectra (400 MHz, D_2O/CD_3CN = 15:1) of **1** at a) 25 ℃ and b) 80 ℃.

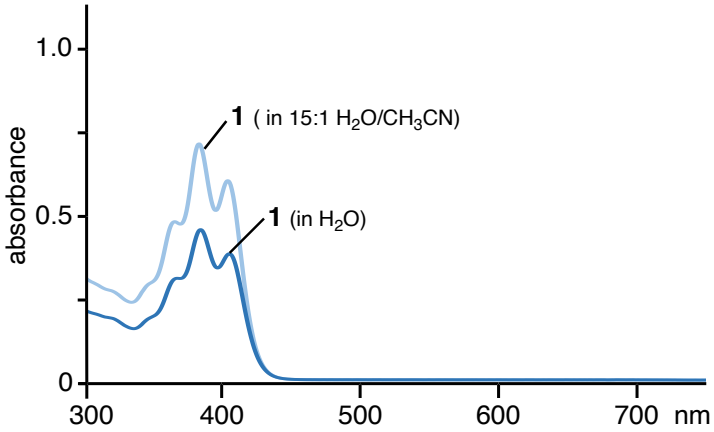

Figure S17. UV-visible spectra (r.t.) of **1** in 15:1 H_2O/CH_3CN (70 μM) and H_2O (43 μM).

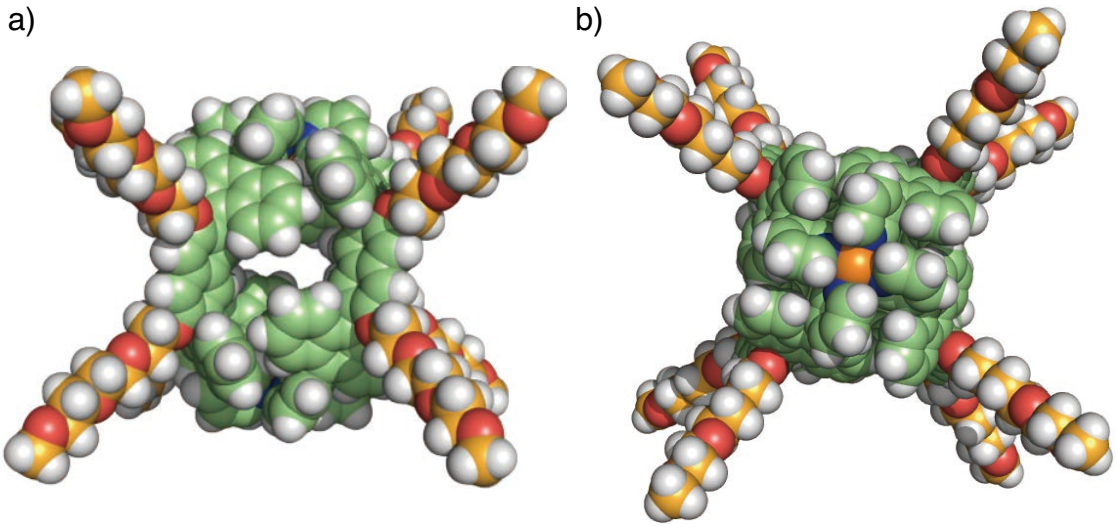

Figure S18. Optimized structure of cage **1** (DFT, CAM-B3LYP/LanL2DZ (for Pt), 6-31G(d,p) (for other atoms) level of theory): a) side and b) top views. The geometry optimization was performed with DFT calculations (Gaussian 16 program package), on the basis of the crystal structure of cage **1'** with short side-chains.[S1]

Formation of caged dyes 1•4a-d MU256, 275, 282, 288, 342

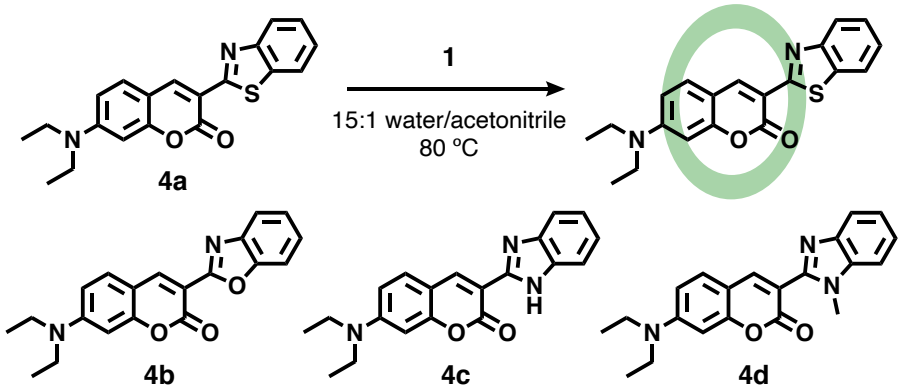

Cage **1** (0.61 mg, 0.14 μmol), 3-(2-benzothiazolyl)-7-(diethylamino)coumarin (**4a**; 0.11 mg, 0.41 μmol), and 15:1 D_2O/CD_3CN (0.45 mL) were added to a glass test tube and then the mixture was stirred at 80 °C for 2 h. The selective formation of 1:1 host-guest complex **1•4a** (50% yield) was confirmed by NMR and UV-visible analyses. In the same way, host-guest complexes **1•4b** (89% yield), **1•4c** (20% yield) and **1•4d** (20% yield) were synthesized using 3-(2-benzoxazolyl)-7-(diethylamino)coumarin (**4b**), 3-(2-benzimidazolyl)-7-(diethylamino)coumarin (**4c**) and 7-(diethylamino)-3-(1-methyl-2-benzimidazolyl)coumarin (**4d**), respectively. The yields of the obtained host-guest complexes (uptake ratios) were estimated by UV-visible analysis (with a calibration curve method) in DMSO, after the removal of suspended unbound dyes by filtration and the lyophilization of the aqueous solutions including cage **1** and its host-guest complexes.

Owing to the insolubility of **4a** in a 15:1 H_2O/CH_3CN solution, the binding constant of **1•4a** was estimated to be ~2.5×10^4 M^{-1} from the UV-visible analysis under high-dilution conditions (0.14 mM to 3.5 μM; Figure S19c).[S4]

1•4a: ESI-TOF MS (15:1 H_2O/CH_3CN): *m/z* 1143.98 [**1•4a** – 4•NO_3^-]$^{4+}$, 1545.93 [**1•4a** – 3•NO_3^-]$^{3+}$.

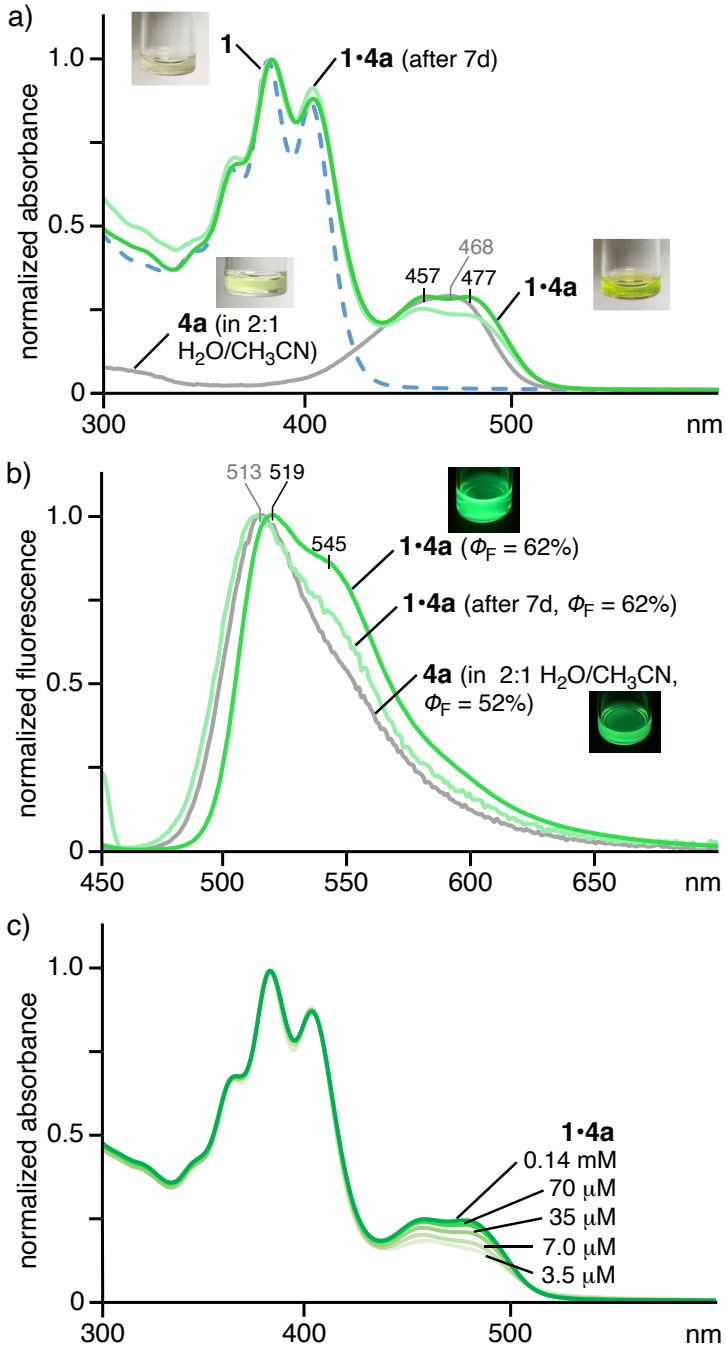

Figure S19. a) UV-visible spectra (r.t.) and photographs of **1•4a** before/after 7 d under ambient conditions (in the dark) in 15:1 H_2O/CH_3CN (0.14 mM based on **1**) and **4a** in 2:1 H_2O/CH_3CN (8 μM) and b) their fluorescence spectra with quantum yields (λ_{ex} = 450 nm) and photographs (λ_{ex} = 365 nm). c) Concentration-dependent UV-visible spectra (r.t.) of **1•4a** in 15:1 H_2O/CH_3CN.

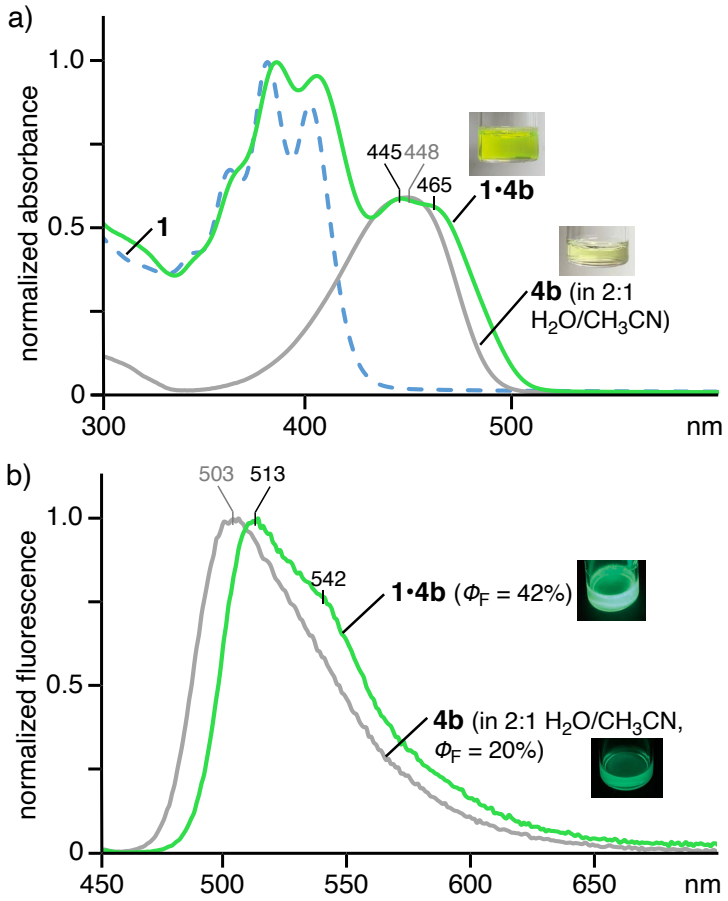

Figure S20. a) UV-visible spectra (r.t.) and photographs of **1•4b** in 15:1 H_2O/CH_3CN (0.14 mM based on **1**) and **4b** in 2:1 H_2O/CH_3CN (8 μM) and b) their fluorescence spectra with quantum yields (λ_{ex} = 450 nm) and photographs (λ_{ex} = 365 nm).

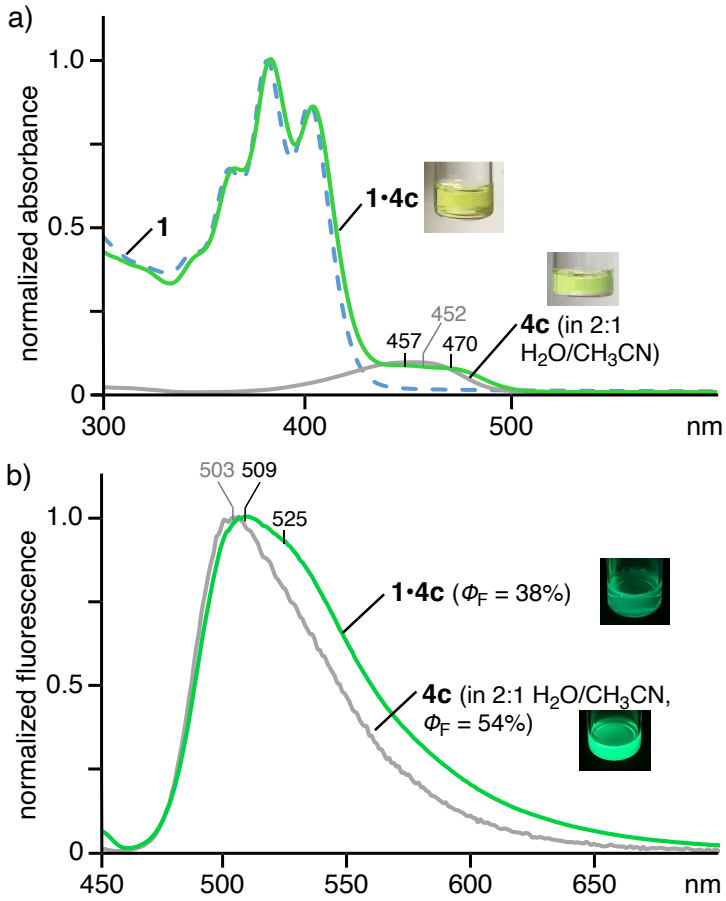

Figure S21. a) UV-visible spectra (r.t.) and photographs of **1•4c** in 15:1 H_2O/CH_3CN (0.14 mM based on **1**) and **4c** in 2:1 H_2O/CH_3CN (8 μM) and b) their fluorescence spectra with quantum yields (λ_{ex} = 450 nm) and photographs (λ_{ex} = 365 nm).

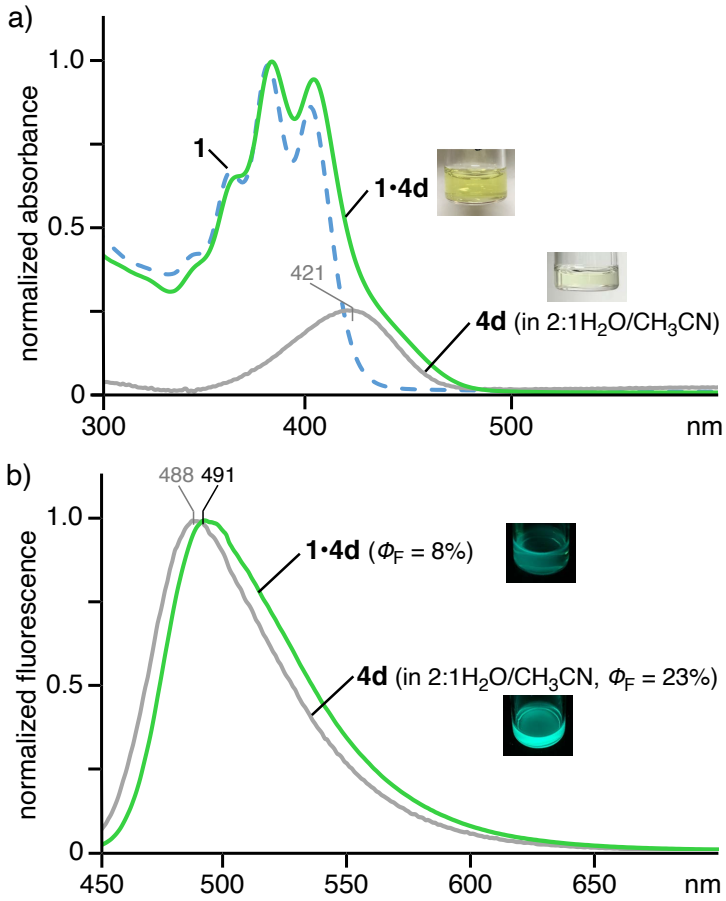

Figure S22. a) UV-visible spectra (r.t.) and photographs of **1•4d** in 15:1 H_2O/CH_3CN (0.14 mM based on **1**) and **4d** in 2:1 H_2O/CH_3CN (8 μM) and b) their fluorescence spectra with quantum yields (λ_{ex} = 429 nm) and photographs (λ_{ex} = 365 nm).

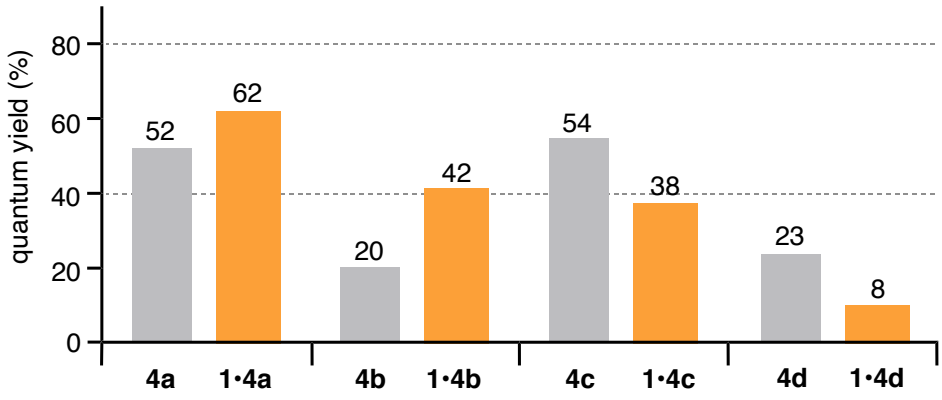

Figure S23. Quantum yields (2:1 H_2O/CH_3CN or 15:1 H_2O/CH_3CN) of **4a**, **4b**, **4c**, and **4d** without/within cage **1**.

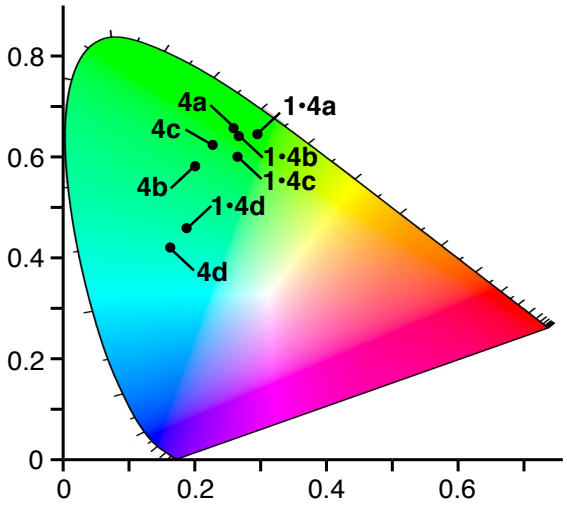

Figure S24. CIE coordinate diagram (2:1 H_2O/CH_3CN or 15:1 H_2O/CH_3CN) of **4a**, **4b**, **4c**, and **4d** without/within cage **1**.

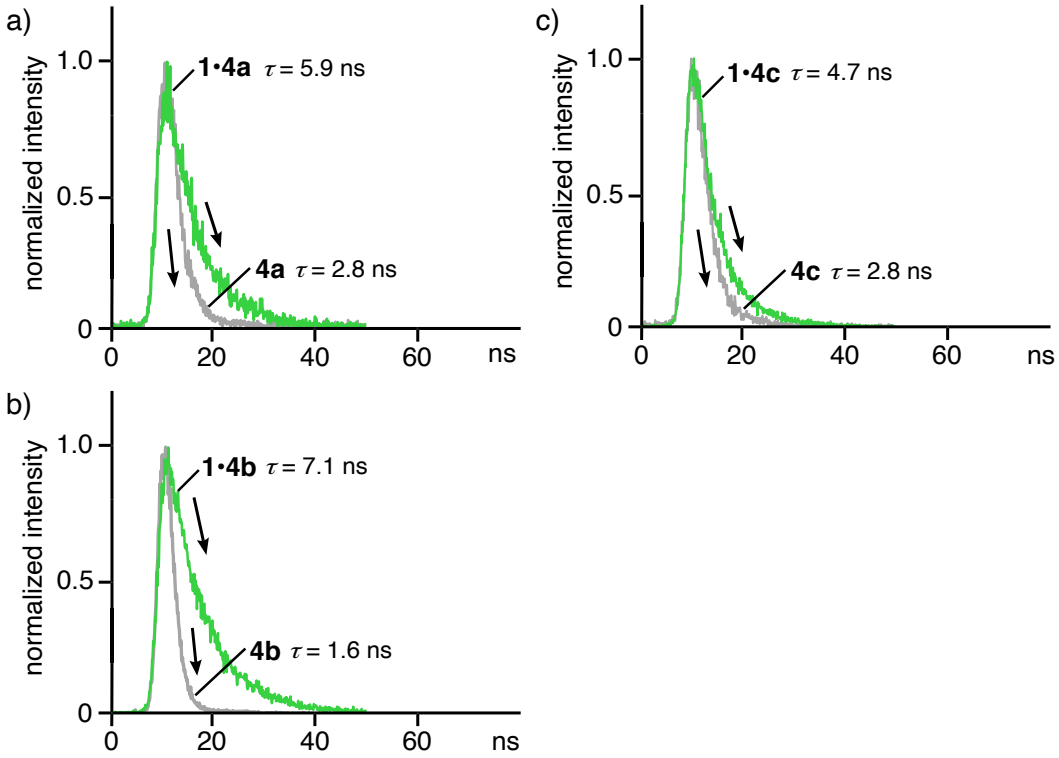

Figure S25. Fluorescence lifetimes (2:1 H_2O/CH_3CN or 15:1 H_2O/CH_3CN, λ_{ex} = 355 nm, r.t.) of a) **4a**, b) **4b**, and c) **4c** without/within cage **1**.

Table S1. Solvent-dependent fluorescence lifetimes and quantum yields of **4a**, **4b**, and **4c** within/without cage **1** in water/acetonitrile (AN) or CH_2Cl_2.

		caged dye 15:1 H_2O/AN[a]	2:1 H_2O/AN[b]	3:1 H_2O/AN[c]	CH_2Cl_2[d]
4a	τ	5.9 ns	2.8 ns	–	3.6 ns
	Φ_F	62%	52%	45%	90%
4b	τ	7.1 ns	1.6 ns	–	3.5 ns
	Φ_F	42%	20%	20%	89%
4c	τ	4.7 ns	2.8 ns	–	4.0 ns
	Φ_F	38%	54%	60%	86%

[a] 70 μM based on **1**. [b] 8.0 μM. [c] 2.0 μM. [d] 40 μM.

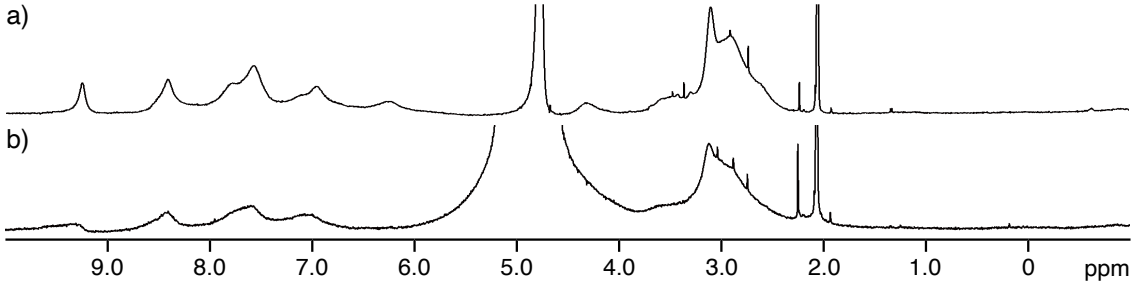

Figure S26a. ^{1}H NMR spectra (500 MHz, 15:1 D_2O/CD_3CN, r.t.) of a) **1** and b) **1•4a**.

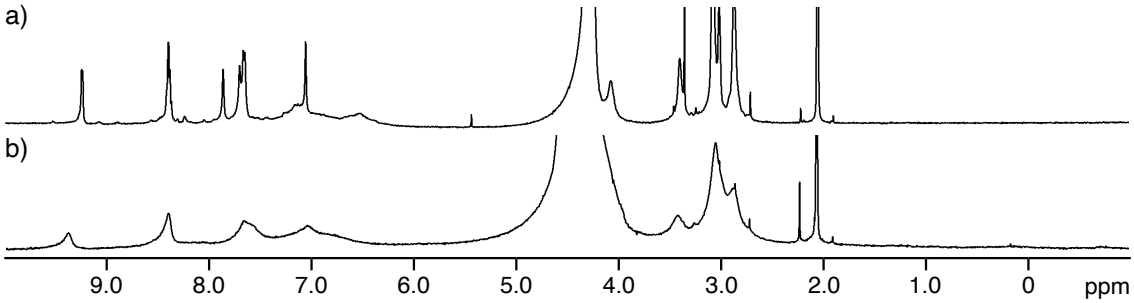

Figure S26b. ^{1}H NMR spectra (500 MHz, 15:1 D_2O/CD_3CN, 75 ºC) of a) **1** and b) **1•4a**.

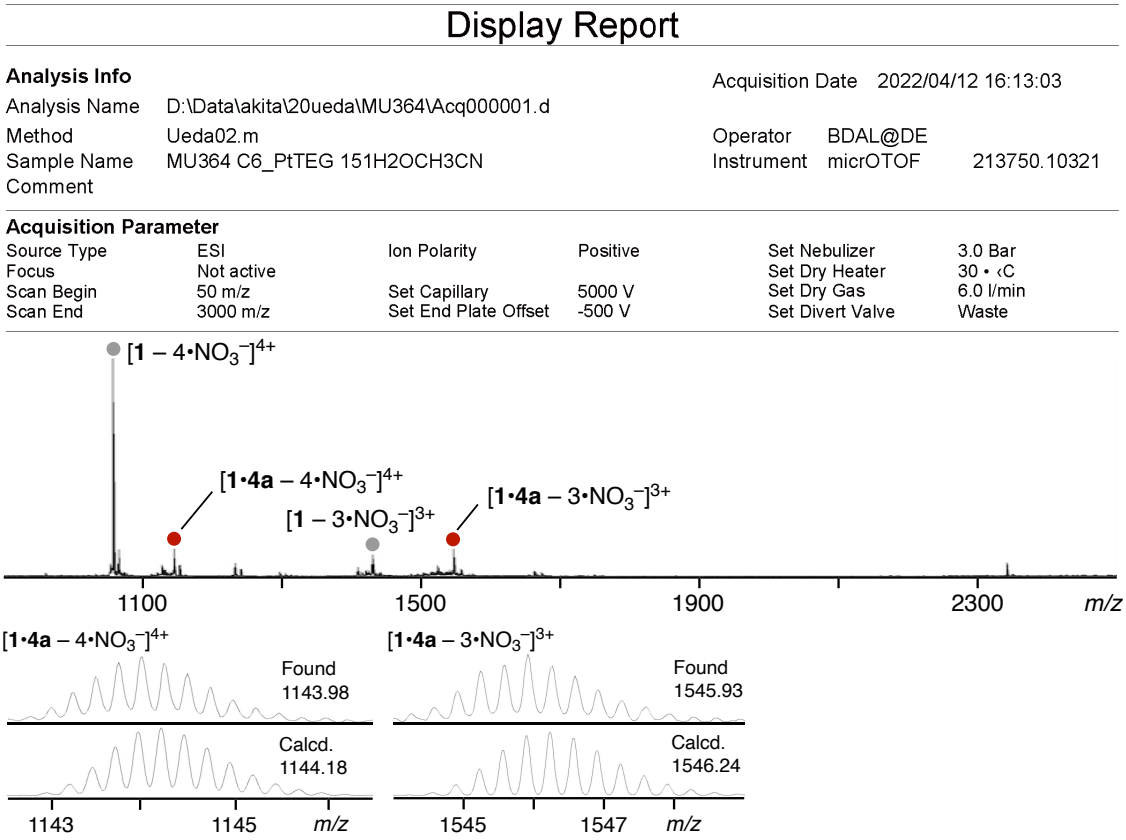

Figure S26c. ESI-TOF MS spectrum (15:1 H_2O/CH_3CN) of **1•4a**.

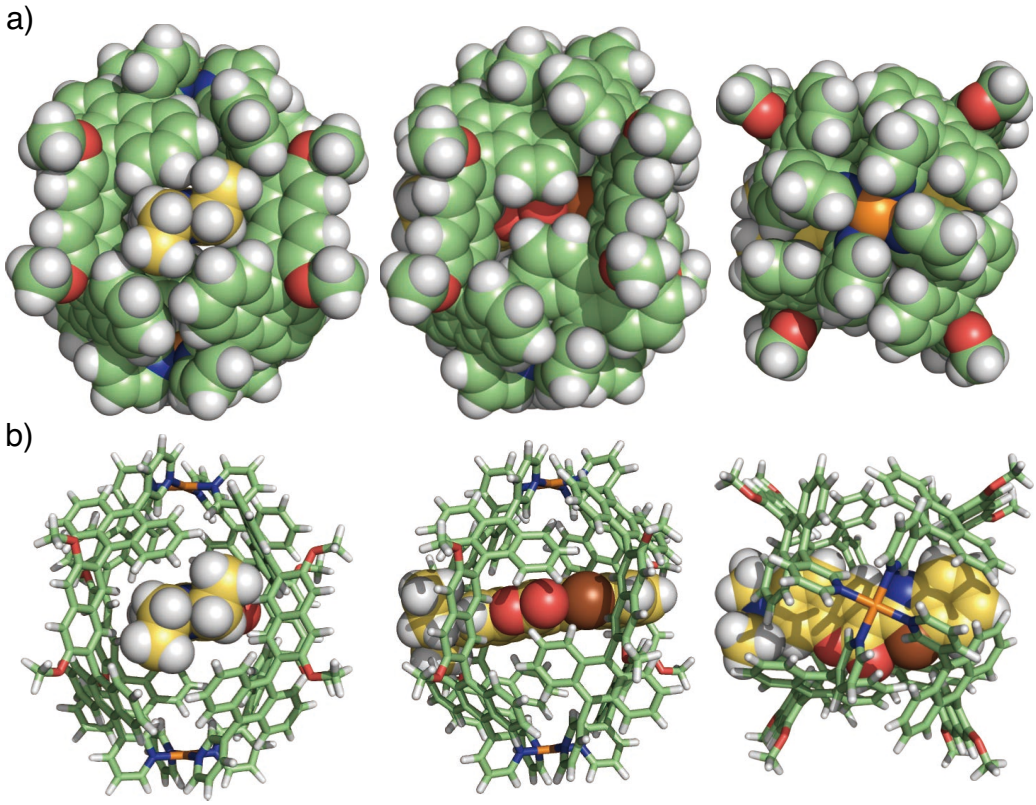

Figure S27a. Optimized structure of **1•4a** (R^1 = -OCH_3): a) space-filling and b) stick/space-filling models. The geometry optimization was performed with molecular mechanics calculations (forcite module, BIOVIA Materials Studio 2020, version 20.1.0.5). On the basis of the crystal structure of cage **1'** with short side-chains,[S1] randomly oriented bulky dye **4a** within cage **1** in several initial structures converged to a threading conformation without host-guest π-stacking interactions.

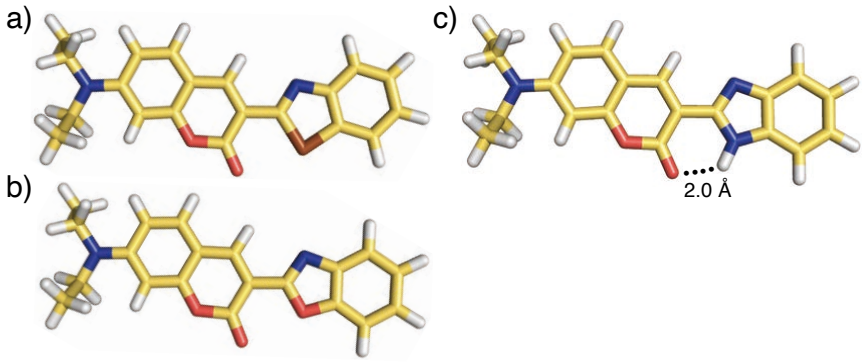

Figure S27b. Optimized structures (DFT, CAM-B3LYP, 6-31G(d,p) level of theory) of a) **4a**, b) **4b**, and c) **4c**.

Formation of caged dyes 1•5a-c MU193, 200, 214, 216, 226

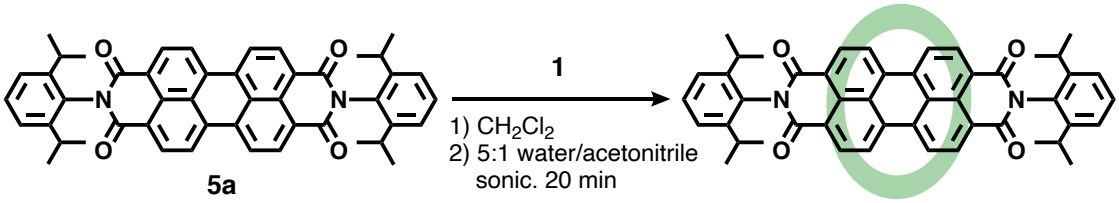

5a

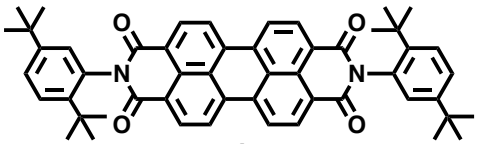

5b

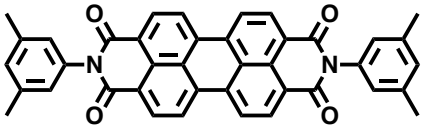

5c

A CH_2Cl_2 solution (1.0 mM) of *N,N'*-bis(2,6-diisopropylphenyl)-3,4,9,10-perylene dicarboximide (**5a**; 0.14 mL, 0.14 μmol) was added to a glass tube including cage **1** (0.61 mg, 0.14 μmol). After evaporation of the solvent, the mixture was sonicated (40 kHz, 150 W) in 5:1 D_2O/CD_3CN (1.0 mL) for 20 min. After the centrifugation and filtration of the resultant suspended solution to remove excess **5a**, the selective formation of 1:1 host-guest complex **1•5a** (48% yield) was confirmed by NMR, MS, DLS, and UV-visible analyses. In the same way, host-guest complexes **1•5b** (20% yield) and **1•5c** were synthesized using *N,N'*-bis(2,5-di-*tert*-butylphenyl)-3,4,9,10-perylenedicarboximide (**5b**) and *N,N'*-bis(3,5-dimethylphenyl)-3,4,9,10-perylenedicarboximide (**5c**), respectively. The yields of the obtained host-guest complexes (uptake ratios) were estimated by UV-visible analysis in DMSO, after the removal of suspended unbound dyes by filtration and the lyophilization of the aqueous solutions including cage **1** and its host-guest complexes.

Owing to the insolubility of **5a** in a 5:1 H_2O/CH_3CN solution, the binding constant of **1•5a** was roughly estimated to be $>10^8$ M^{-1} from the UV-visible analysis under high-dilution conditions (70 to 3.5 μM; Figure S28c).[S4]

1•5a: ESI-TOF MS (5:1 H_2O/CH_3CN): *m/z* 1233.97 [**1•5a** – 4•NO_3^-]$^{4+}$, 1665.91 [**1•5a** – 3•NO_3^-]$^{3+}$.

1•5b: ESI-TOF MS (5:1 H_2O/CH_3CN): *m/z* 1248.01 [**1•5b** – 4•NO_3^-]$^{4+}$, 1684.63 [**1•5b** – 3•NO_3^-]$^{3+}$.

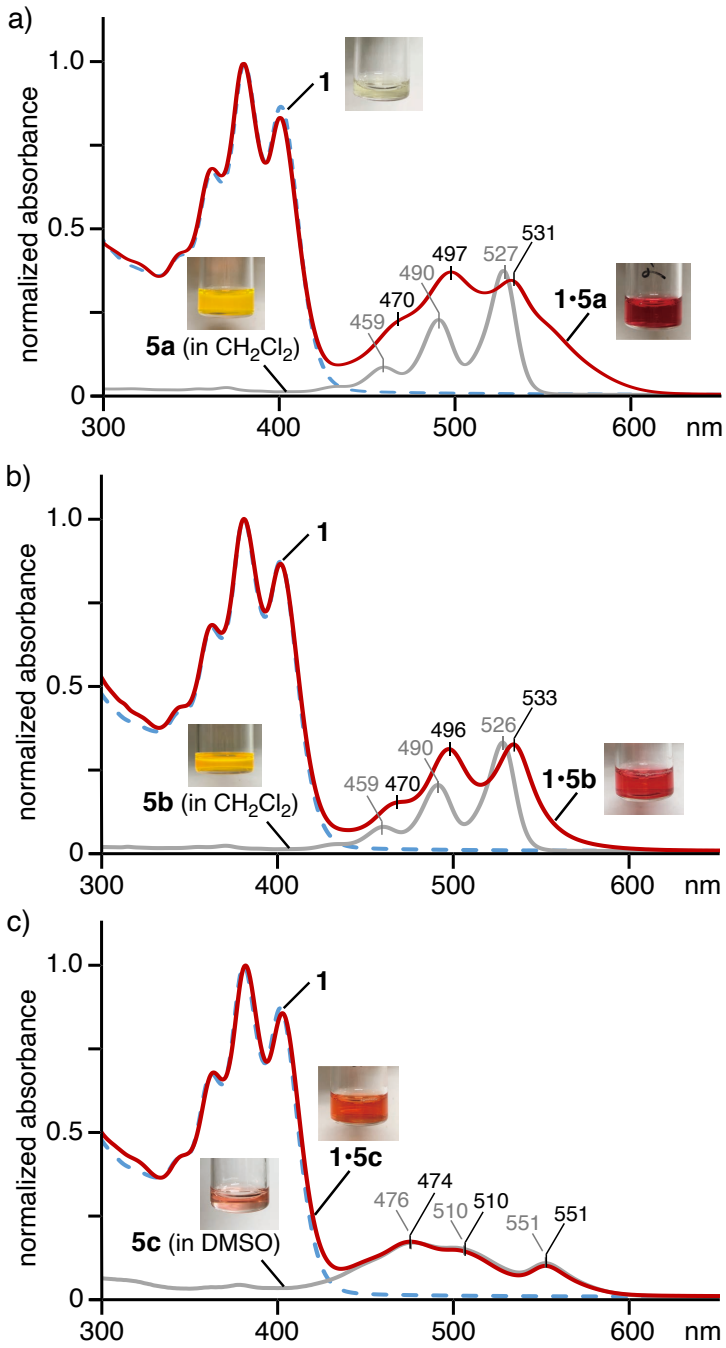

Figure S28a. UV-visible spectra (5:1 H_2O/CH_3CN, 0.14 mM based on **1**, r.t.) and photographs of a) **1•5a**, **1**, and **5a** in CH_2Cl_2, b) **1•5b**, **1**, and **5b** in CH_2Cl_2, and c) **1•5c**, **1**, and **5c** in DMSO.

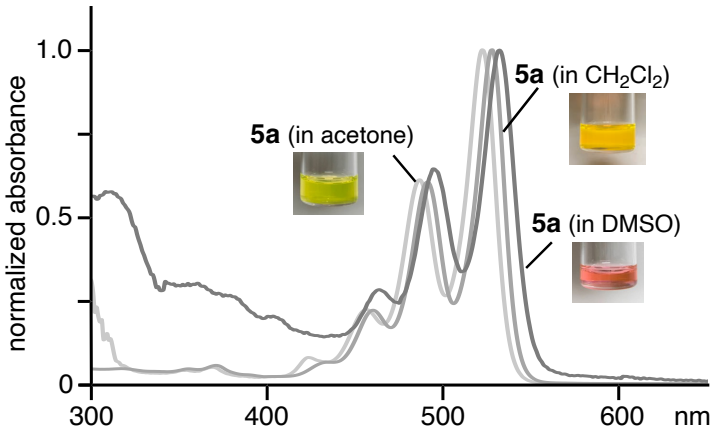

Figure S28b. UV-visible spectra (70 μM, r.t.) and photographs of **5a** in CH_2Cl_2, acetone, and DMSO.

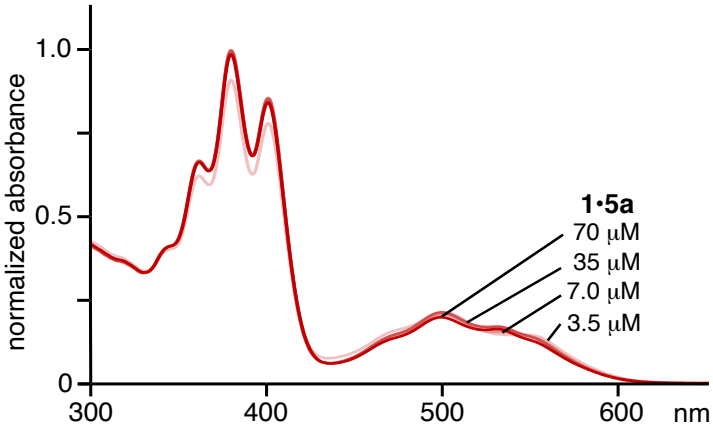

Figure S28c. Concentration-dependent UV-visible spectra (r.t.) of **1•5a** in 5:1 H_2O/CH_3CN.

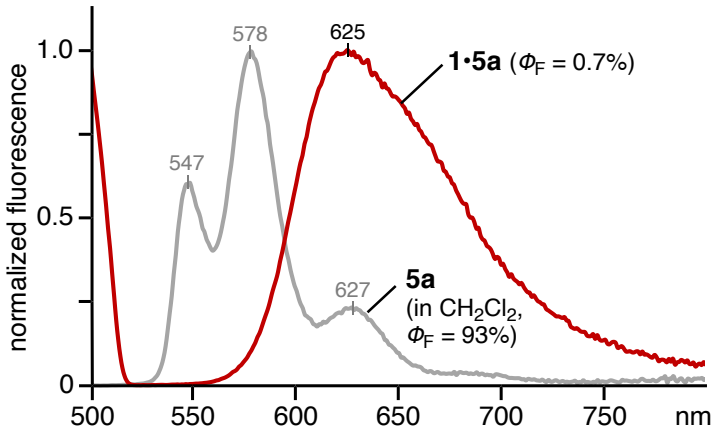

Figure S29. Fluorescence spectra (λ_{ex} = 500 nm, 70 μM, r.t.) and quantum yields of **1•5a** in 5:1 H_2O/CH_3CN and **5a** in CH_2Cl_2.

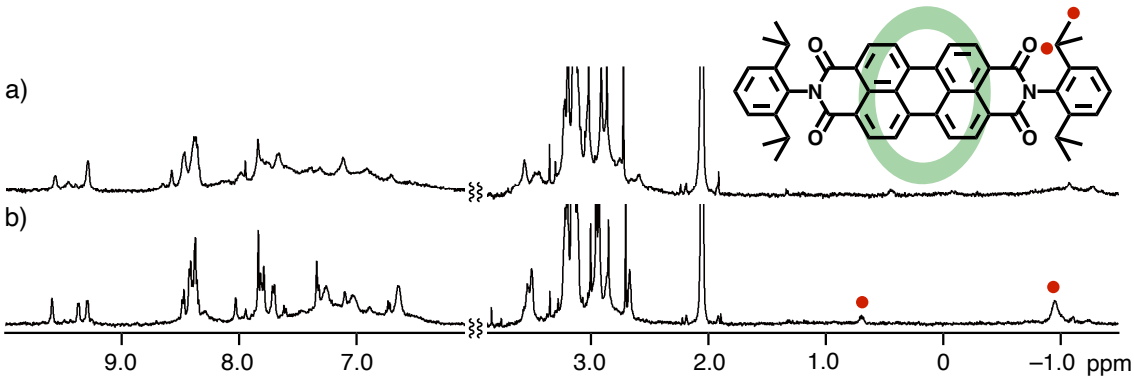

Figure S30. ^{1}H NMR spectra (500 MHz, 5:1 D_2O/CD_3CN) of **1•5a** at a) 25 °C and b) 75 °C.

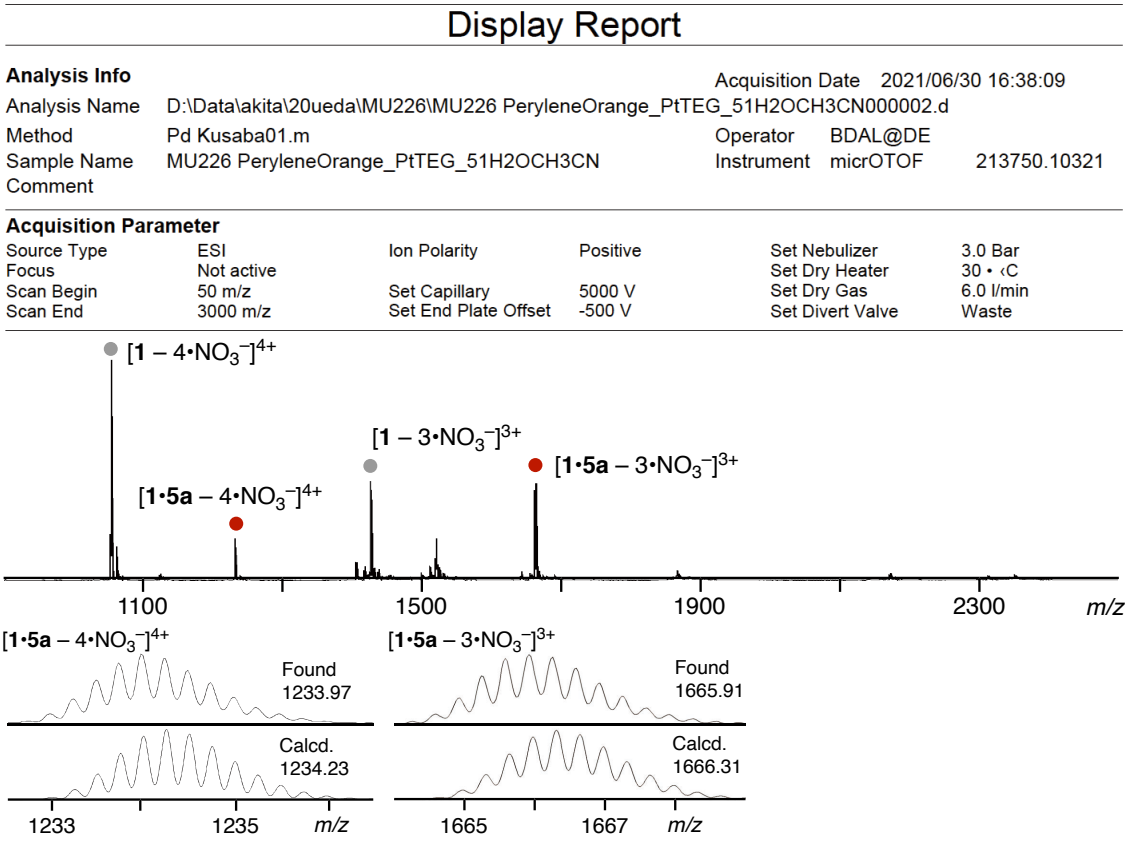

Figure S31. ESI-TOF MS spectrum (5:1 H_2O/CH_3CN) of **1•5a**.

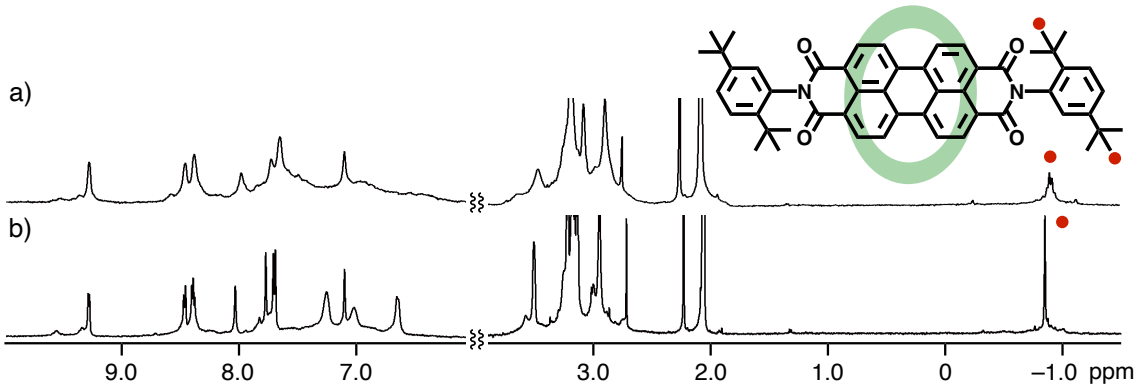

Figure S32a. ^{1}H NMR spectra (500 MHz, 5:1 D_2O/CD_3CN) of **1•5b** at a) 25 ºC and b) 75 ºC.

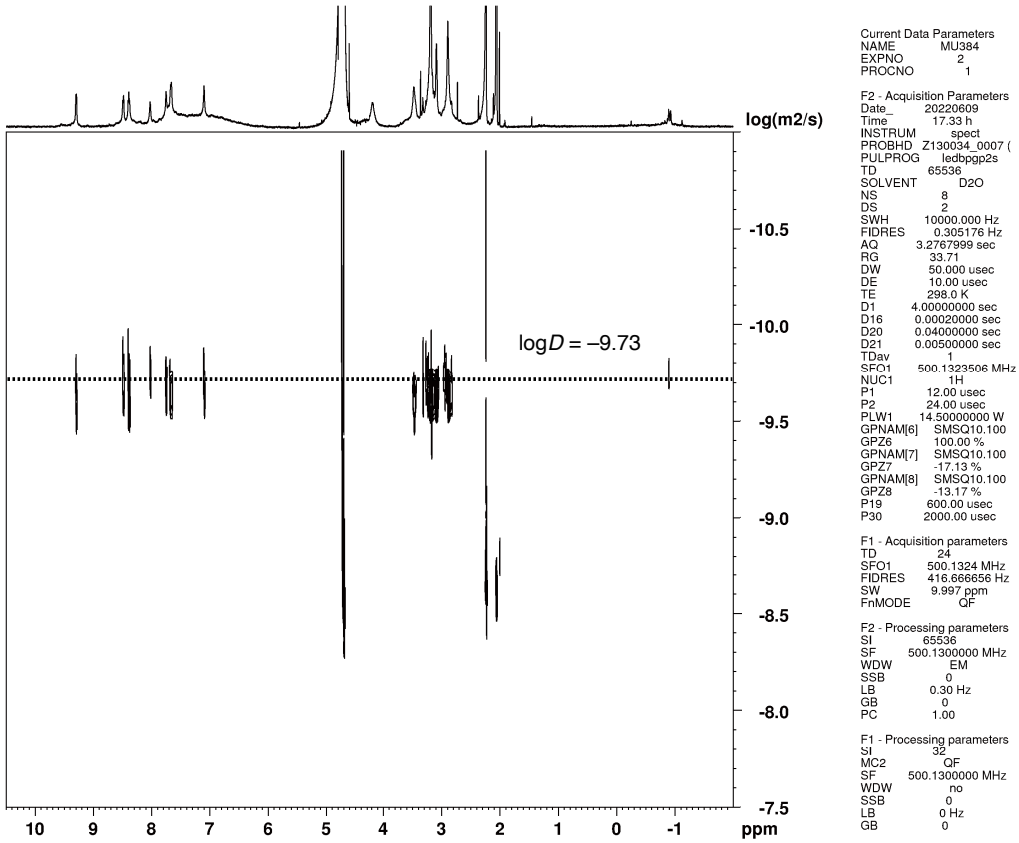

Figure S32b. ^{1}H DOSY NMR (500 MHz, 5:1 D_2O/CD_3CN, 25 ºC) of **1•5b**.

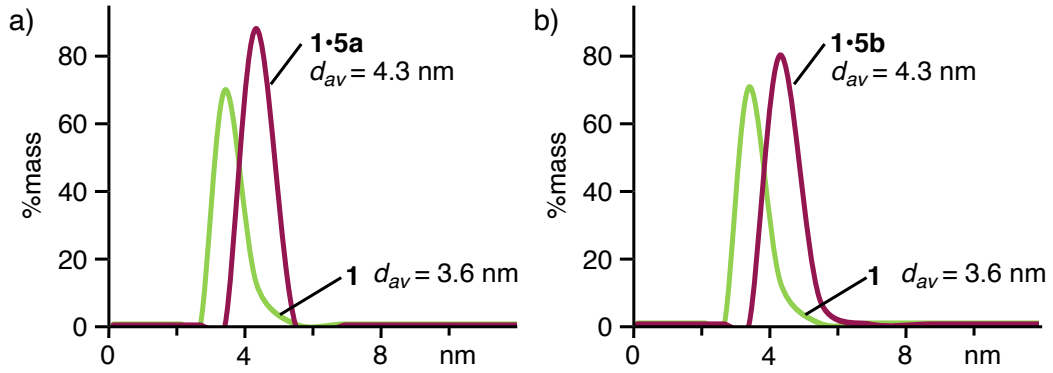

Figure S32c. Particle number-size distribution of a) **1•5a** and b) **1•5b** by DLS analysis (5:1 H_2O/CH_3CN, 0.14 mM based on **1**, 25 ºC).

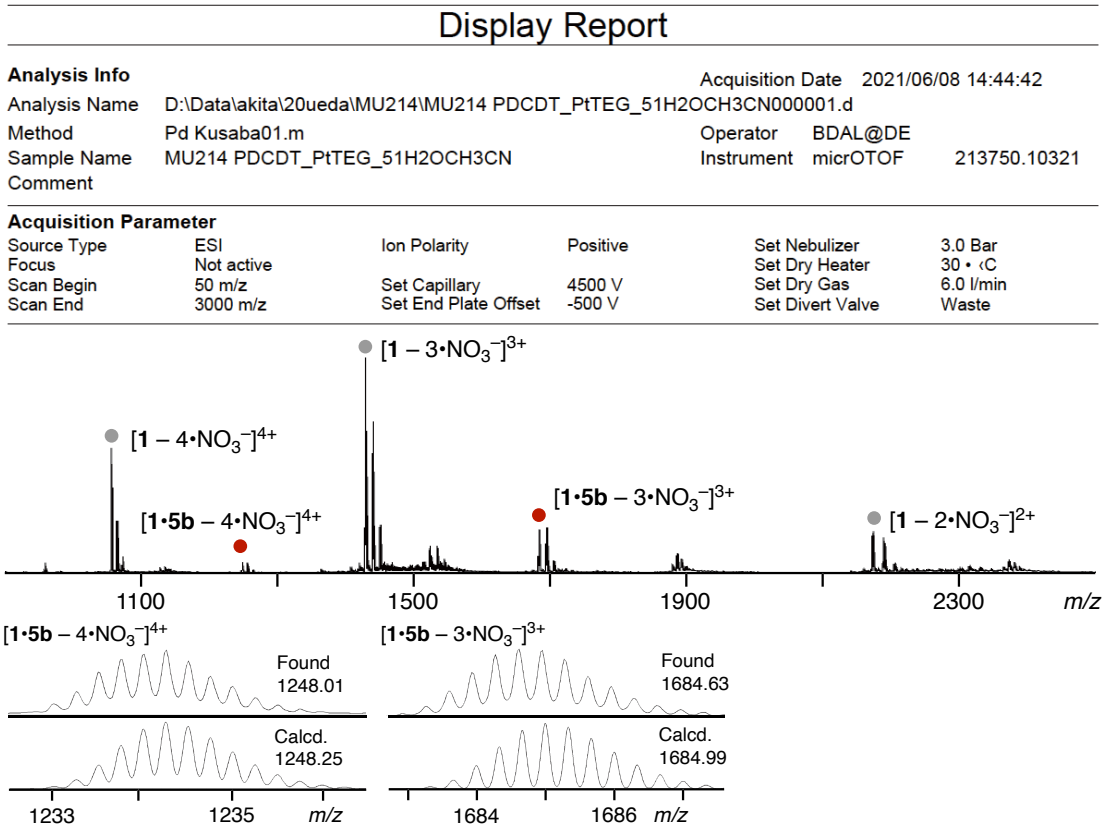

Figure S33. ESI-TOF MS spectrum (5:1 H_2O/CH_3CN) of **1•5b**.

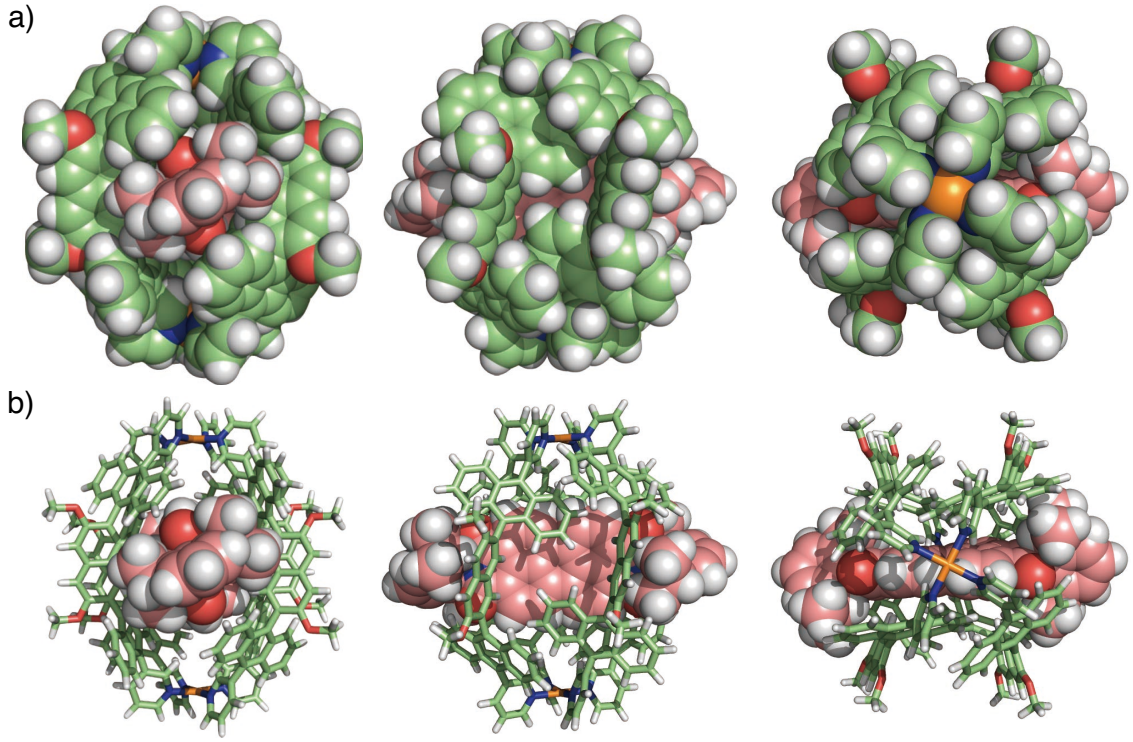

Figure S34. Optimized structure of **1•5a** (R^1 = -OCH_3): a) space-filling and b) stick/space-filling models. The geometry optimization was performed with molecular mechanics calculations (forcite module, BIOVIA Materials Studio 2020, version 20.1.0.5). On the basis of the crystal structure of cage **1'** with short side-chains,[S1] randomly oriented bulky dye **5a** within cage **1** in several initial structures converged to a threading conformation without host-guest π-stacking interactions.

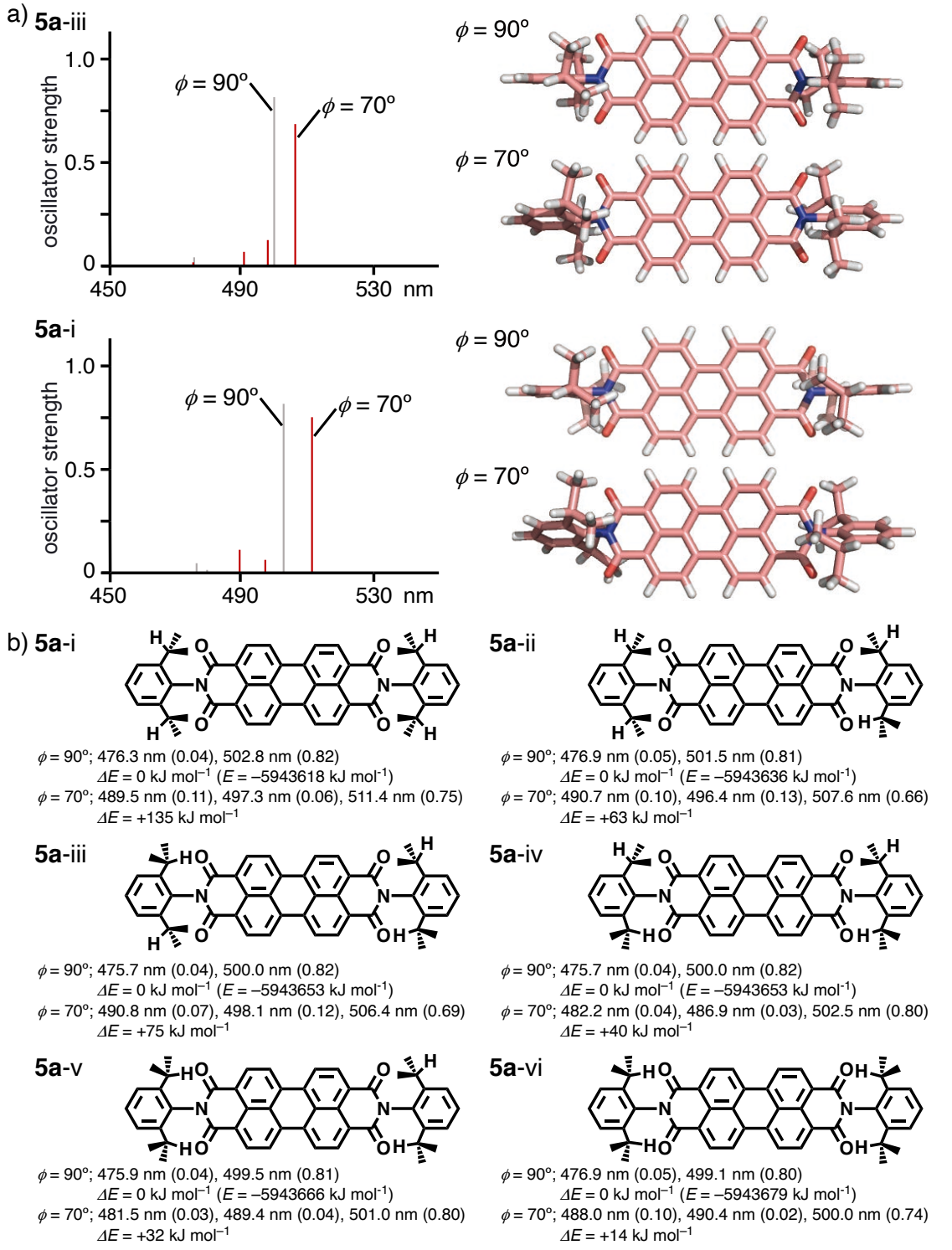

Figure S35a. a) Predicted UV-visible spectra and molecular modeling of **5a** with different dihedral angles (ϕ) between the phenyl and imide rings and b) their predicted, electronic absorption bands (oscillator strength) and energies. The predicted absorption bands were obtained by TD-DFT calculation (B3LYP/6-31G(d) level of theory). The optimized structures (ϕ = 90° and 70°) and energies were obtained by DFT calculation of **5a** (CAM-B3LYP, 6-31G(d,p) level of theory). The torsional structures were created in GaussView 6. DFT/TD-DFT calculations were performed with Gaussian 16 program package.

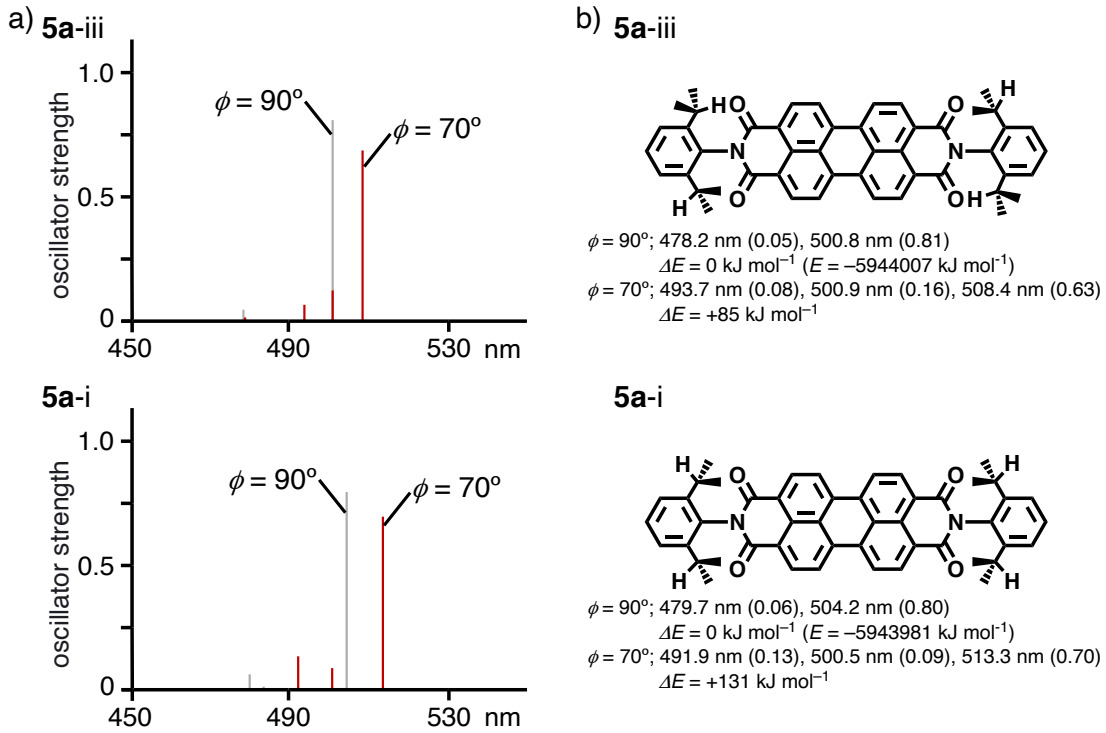

Figure S35b. a) Predicted UV-visible spectra of representative isomers **5a**-iii and **5a**-i with dihedral angles ϕ = 90º and 70º and b) their predicted, electronic absorption bands (oscillator strength) and energies. The predicted absorption bands were obtained by TD-DFT calculation (B3LYP+D3BJ/6-31G(d) level of theory) and the energies were obtained by DFT calculation (CAM-B3LYP+D3BJ/6-31G(d,p) level of theory), using the optimized structures of **5a**-iii and **5a**-i obtained in Figure S35a. DFT/TD-DFT calculations were performed with Gaussian 16 program package.

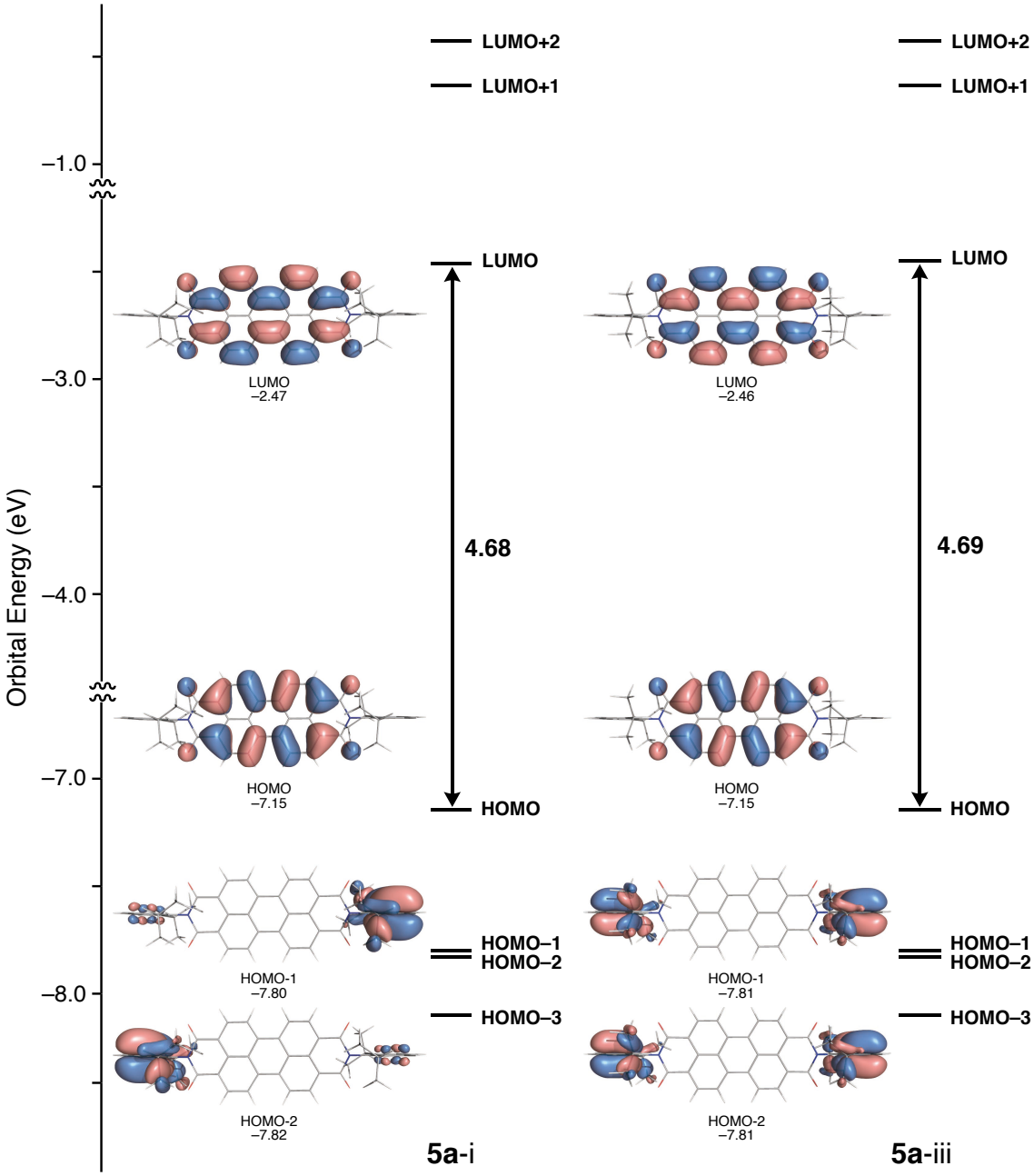

Figure S36. Energy diagrams and molecular orbitals of **5a** (ϕ = 90º), estimated by DFT calculation (CAM-B3LYP, 6-31G(d,p) level of theory).

Formation of caged dyes 1•6a-e MU145, 151, 158, 163, 203, 336, 343, 347, 349, 350

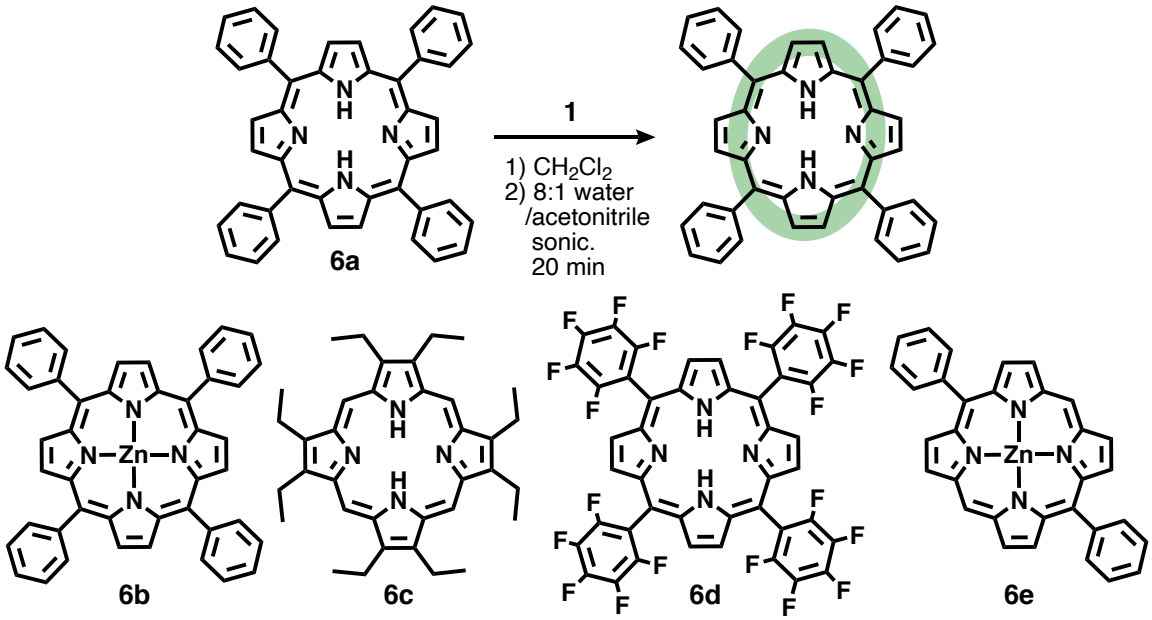

A CH_2Cl_2 solution (1.0 mM) of tetraphenylporphyrin **6a** (0.14 mL, 0.14 μmol) was added to a glass tube including cage **1** (0.61 mg, 0.14 μmol). After evaporation of the solvent, the mixture was sonicated in 8:1 H_2O/CH_3CN (1.0 mL) for 20 min (40 kHz, 150 W). After the removal of excess **6a** by centrifugation and filtration, the formation of 1:1 host-guest complex **1•6a** (70% yield) was confirmed by UV-visible analysis. In the same way, 1:1 host-guest complexes **1•6b** (90% yield), **1•6c** (40% yield), **1•6d** (80% yield), and **1•6e** (70% yield) were synthesized using Zn(II)-tetraphenylporphyrin (**6b**), octaethylporphyrin (**6c**), tetrakis(pentafluorophenyl)- porphyrin (**6d**), and Zn(II)-diphenylporphyrin (**6e**), respectively. The yields of the obtained host-guest complexes (uptake ratios) were estimated by UV-visible analysis (with a calibration curve method) in DMSO, after the removal of suspended unbound dyes by filtration and the lyophilization of the aqueous solutions including cage **1** and its host-guest complexes.

Owing to the insolubility of **6a** in a 8:1 H_2O/CH_3CN solution, the binding constant of **1•6a** was roughly estimated to be $>10^8$ M^{-1} from the UV-visible analysis under high-dilution conditions (70 to 3.5 μM; Figure S39c).[S4]

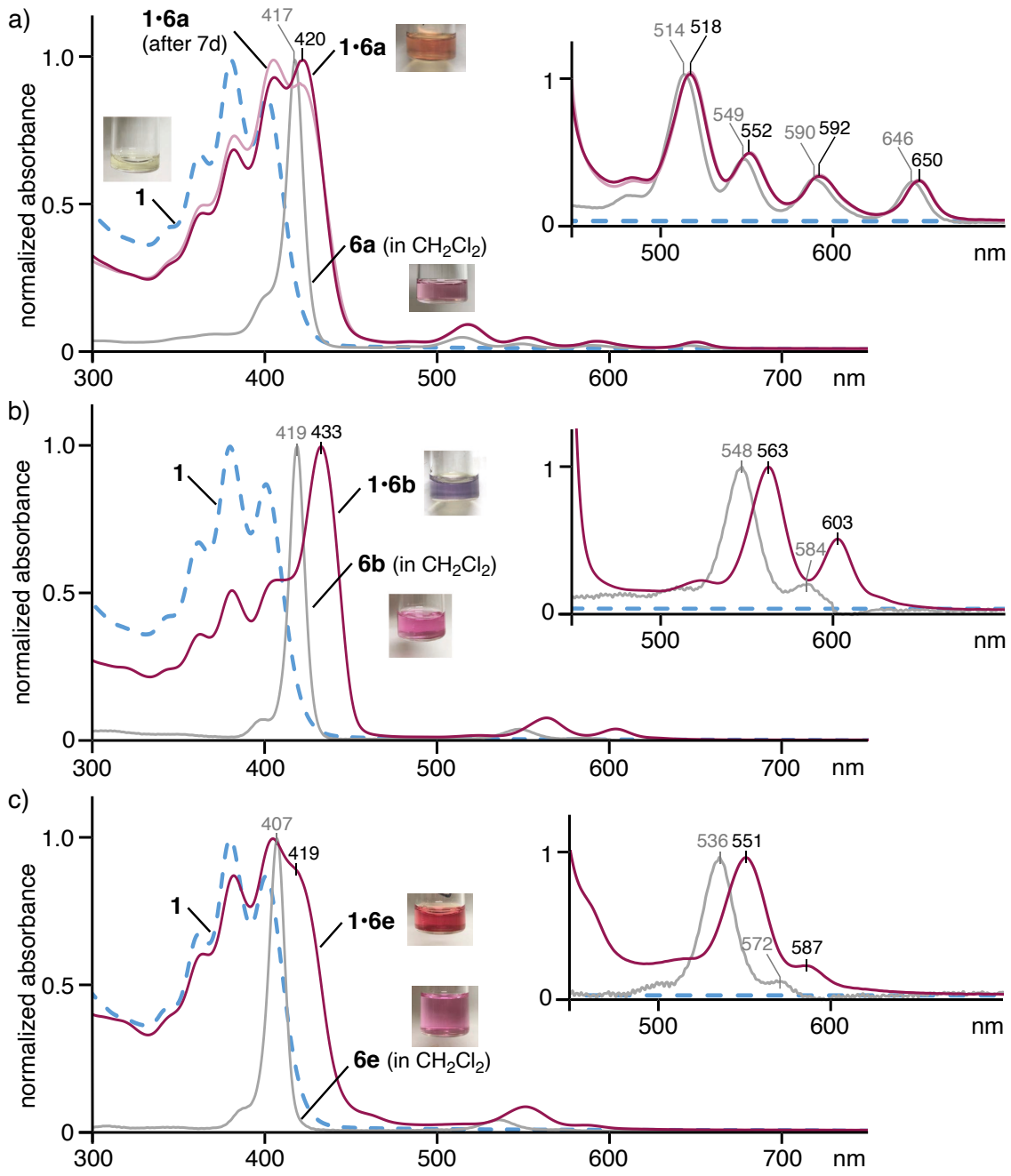

Figure S37a. UV-visible spectra and photographs (r.t., 8:1 H_2O/CH_3CN, 0.14 mM based on **1**) of a) **1•6a** before/after 7 d under ambient conditions, **1**, and **6a** in CH_2Cl_2, b) **1•6b**, **1**, and **6b** in CH_2Cl_2, c) **1•6e**, **1**, and **6e** in CH_2Cl_2.

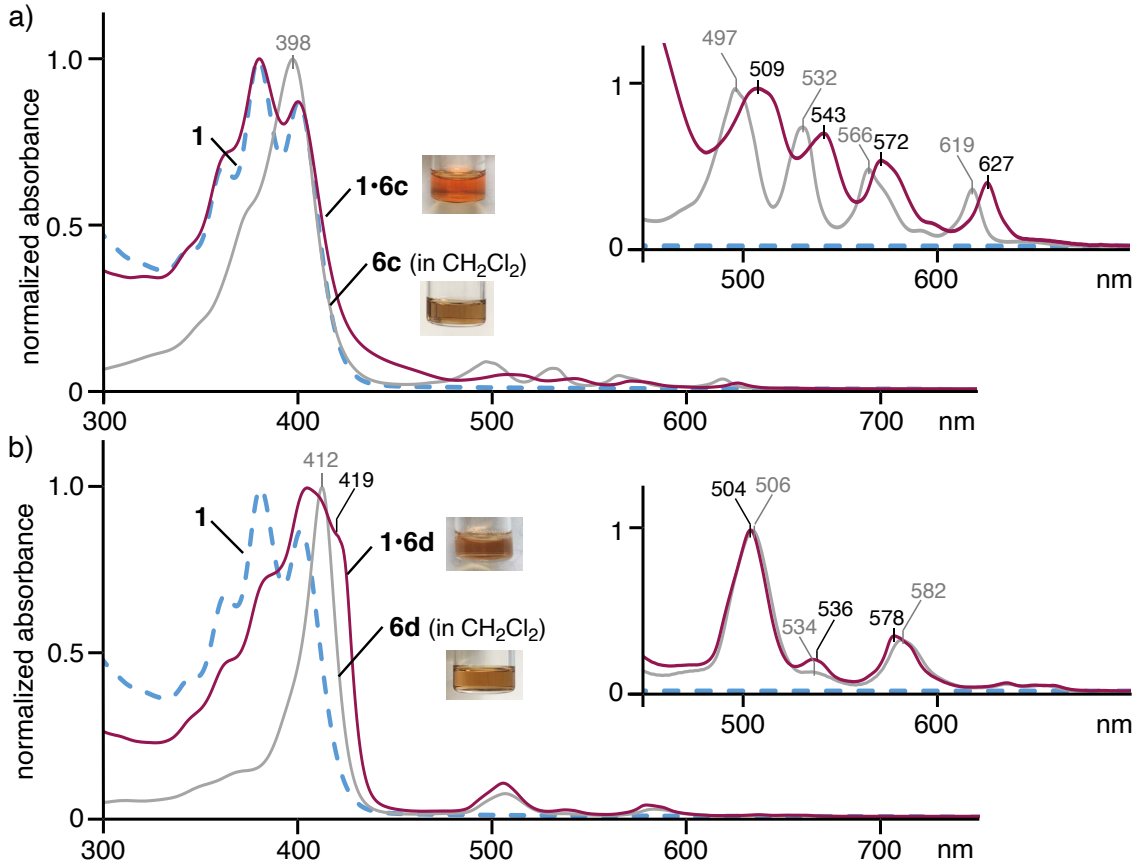

Figure S37b. UV-visible spectra and photographs (r.t., 8:1 H_2O/CH_3CN, 0.14 mM based on **1**) of a) **1•6c**, **1**, and **6c** in CH_2Cl_2, b) **1•6d**, **1**, and **6d** in CH_2Cl_2.

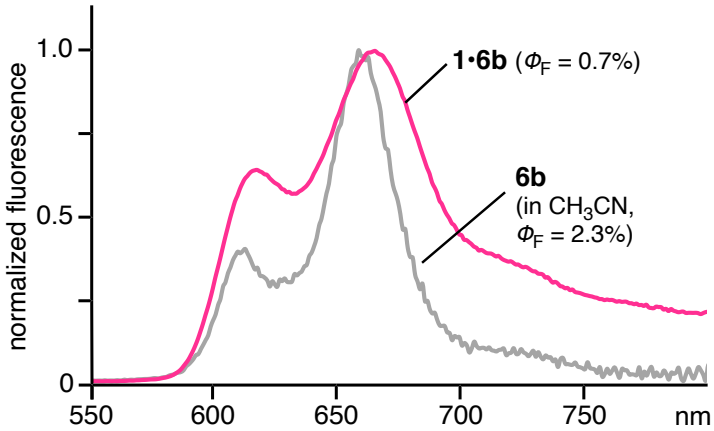

Figure S38. Fluorescence spectra (λ_{ex} = 429 nm, r.t., 70 μM) and quantum yields of **1•6b** in 8:1 H_2O/CH_3CN and **6b** (70 μM) in CH_3CN.

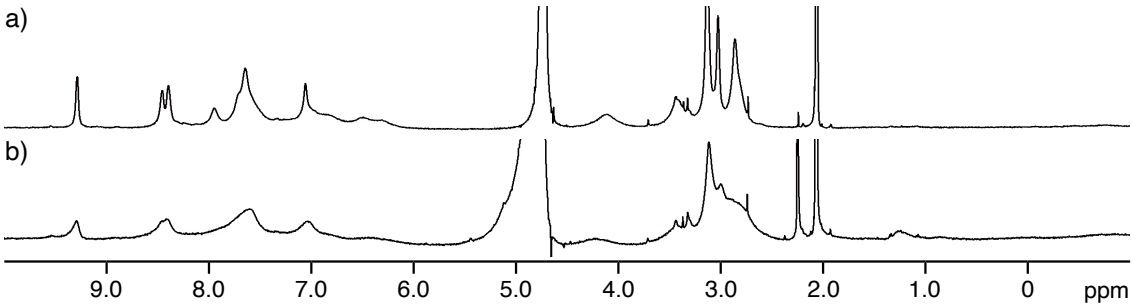

Figure S39a. ^{1}H NMR spectra (500 MHz, 8:1 D_2O/CD_3CN, r.t.) of a) **1** and b) **1•6a**.

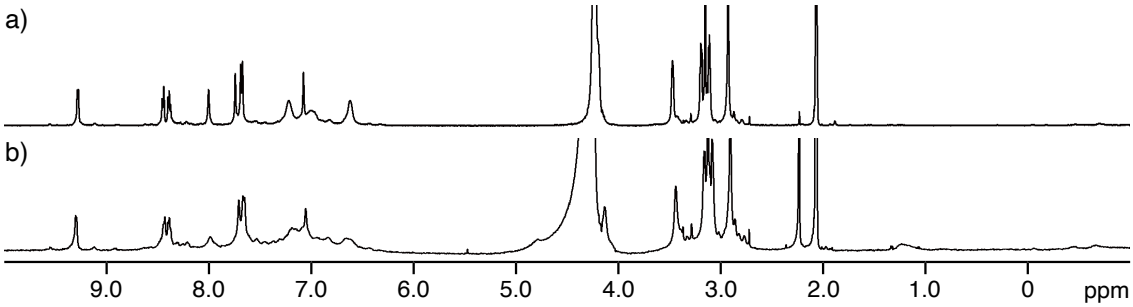

Figure S39b. ^{1}H NMR spectra (500 MHz, 8:1 D_2O/CD_3CN, 75 ºC) of a) **1** and b) **1•6a**.

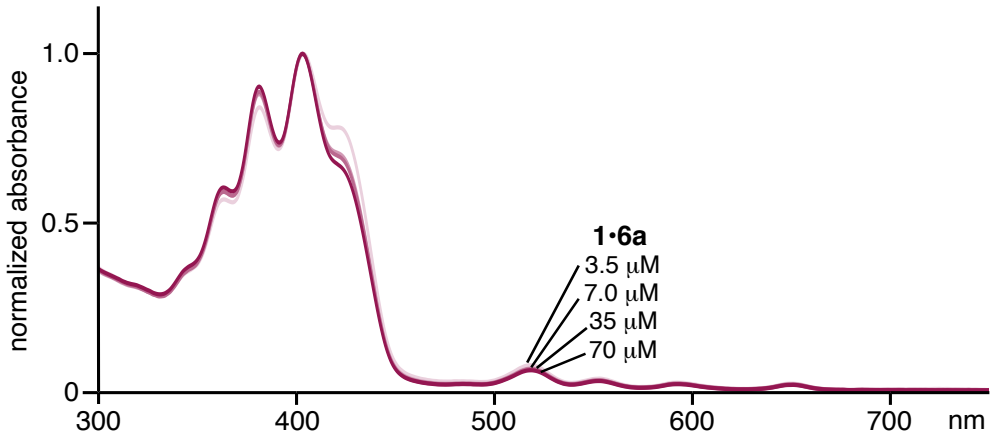

Figure S39c. Concentration-dependent UV-visible spectra (r.t.) of **1•6a** in 8:1 H_2O/CH_3CN.

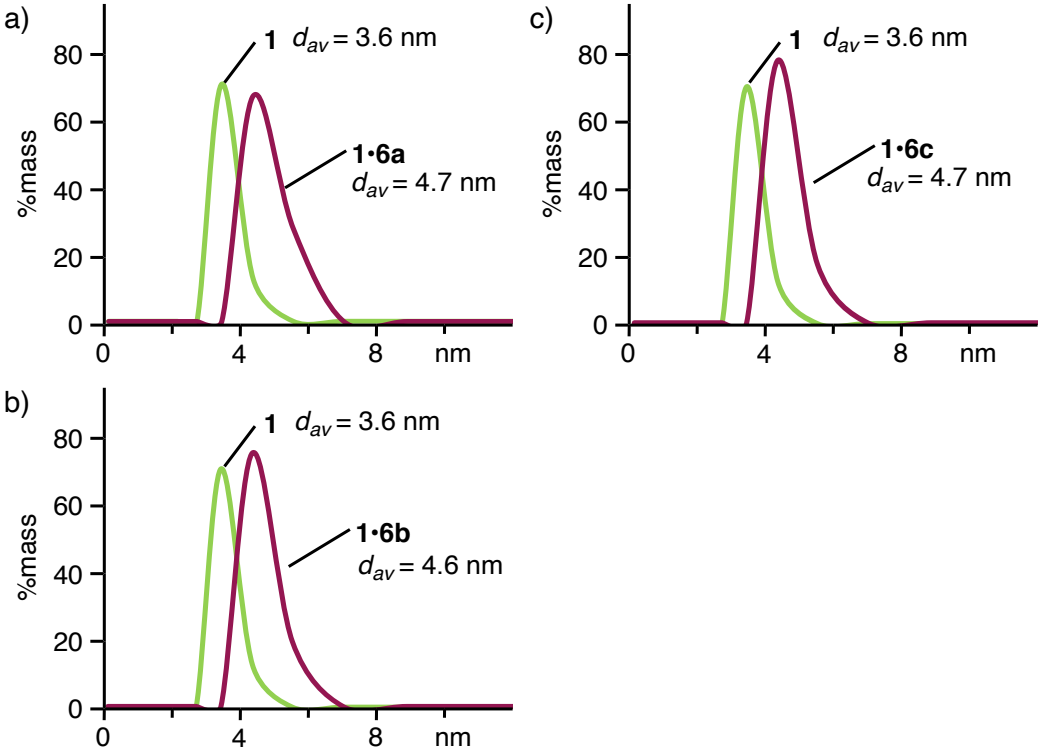

Figure S40. Particle number-size distribution of a) **1•6a**, b) **1•6b**, and c) **1•6c** by DLS analysis (8:1 H_2O/CH_3CN, 0.14 mM based on **1**, 25 ºC).

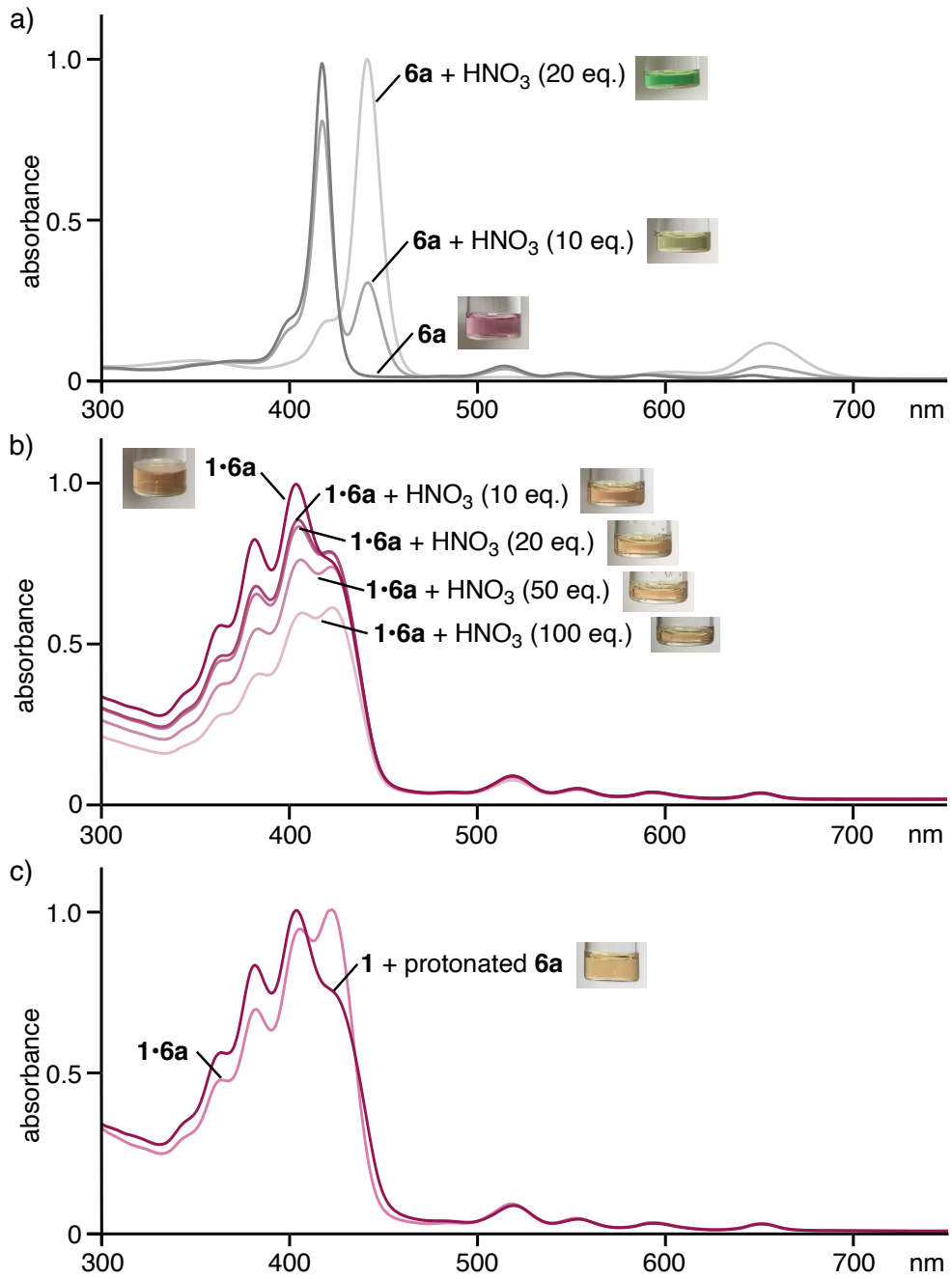

Figure S41a. UV-visible spectra and photographs (r.t., 8:1 H_2O/CH_3CN, 70 μM based on **1**) of a) **6a** in CH_2Cl_2 and b) **1•6a** after HNO_3 addition. c) UV-visible spectra and a photograph (r.t., 8:1 H_2O/CH_3CN, 0.14 mM based on **1**) of **1•6a** and **1** after the addition of protonated **6a** with HNO_3 (50 eq. based on **1**).

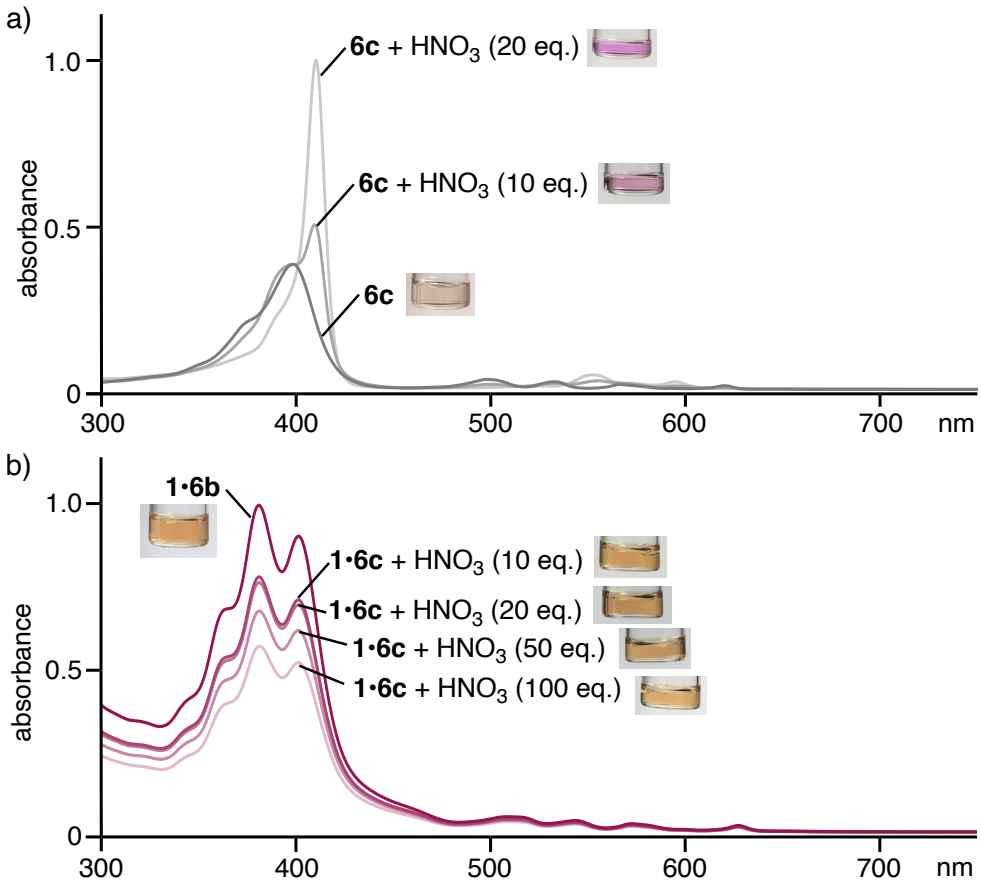

Figure S41b. UV-visible spectra and photographs (r.t., 8:1 H_2O/CH_3CN, 70 μM based on **1**) of a) **6c** in CH_2Cl_2 and b) **1•6c** after HNO_3 addition.

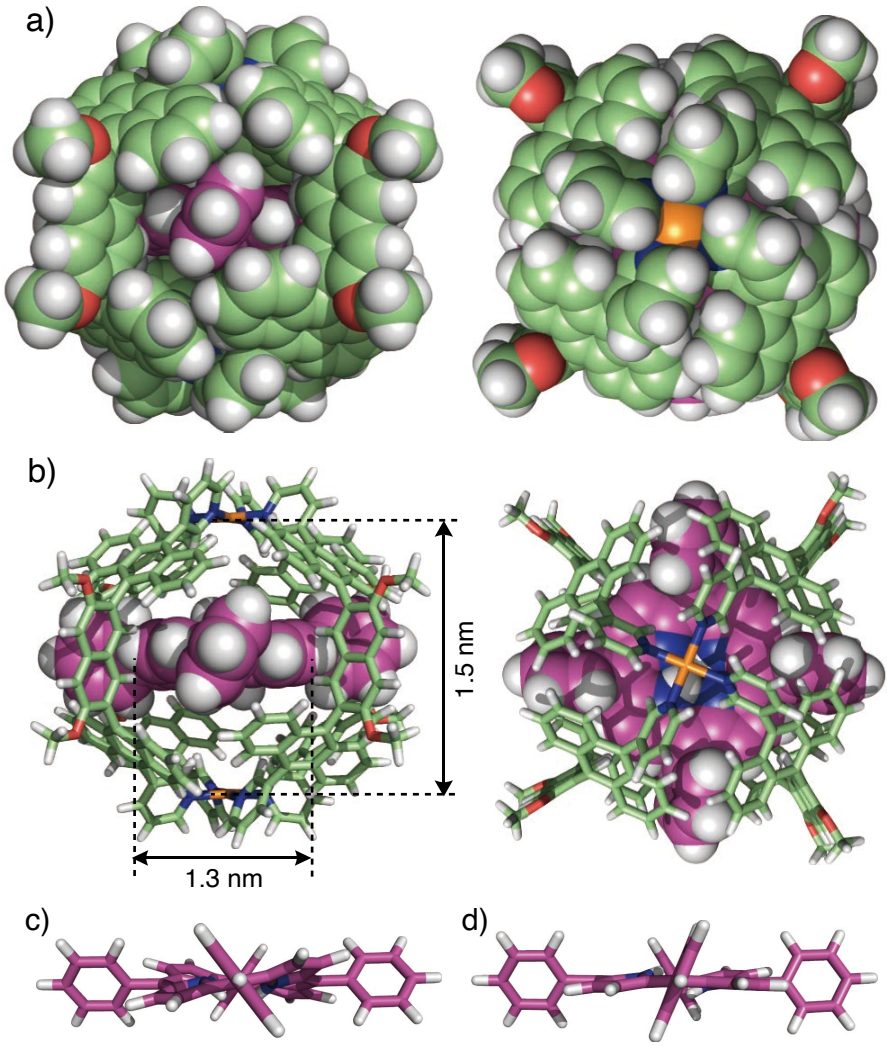

Figure S42. Optimized structure of **1•6a** ($R^1 = OCH_3$): a) space-filling and b) stick/space-filling models. Optimized structures of c) free **6a** and d) **6a** within cage **1** (the cage framework is omitted for clarity). The geometry optimization was performed with MM calculations (forcite module, BIOVIA Materials Studio 2020, version 20.1.0.5). On the basis of the crystal structure of cage **1'** with short side-chains,[S1] randomly oriented bulky dye **6a** within cage **1** in several initial structures converged to a threading conformation without host-guest π-stacking interactions.

Table S2. Energies of neutral dye **6a** and cationic dye **6a'** within/without cage **1**

	$E_H + E_G$[a] [kJ mol^{-1}]	$E_{H•G}$[b] [kJ mol^{-1}]	ΔE[c] [kJ mol^{-1}]	method[d]
6a	3792.67	3770.24	–22.43	MM
6a'	4148.02	5275.48	+1127.46	MM
	7983.21	8880.23	+897.02	PM6

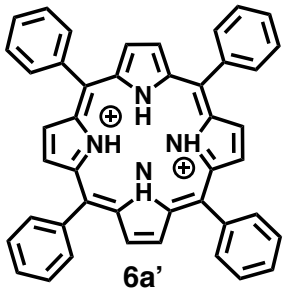

6a'

[a] E_{H+G}: energy of free **6** and cage **1**. [b] $E_{H•G}$: energy of **6** within cage **1**. [c] Determined by $E_{H•G} - (E_H + E_G)$. [d] The calculated energies were obtained by MM (forcite module, BIOVIA Materials

Studio 2020, version 20.1.0.5) and PM6 calculations, from randomly oriented bulky dyes **6** and **6a'** within cage **1** in several initial structures.

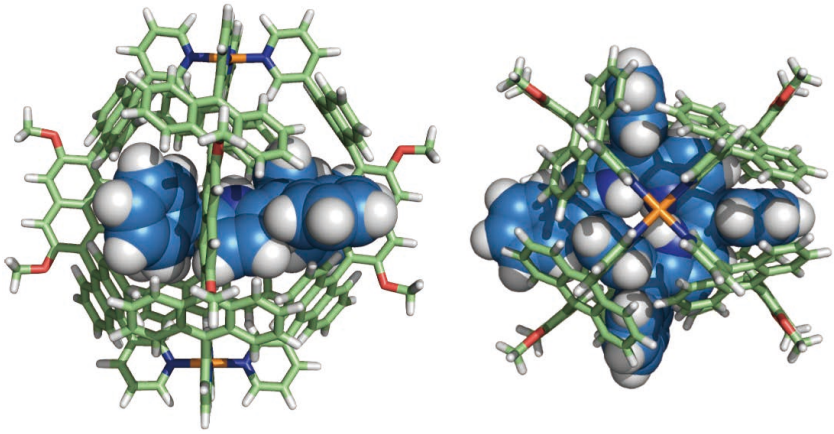

Figure S43. Optimized structure of **1•6a'** (R^1 = OCH_3): side and top views. The geometry optimization was performed with PM6 calculation. On the basis of the crystal structure of cage **1'** with short side-chains,[S1] randomly oriented cationic dye **6a'** within cage **1** in several initial structures converged to a distorted host-guest structure.

Competitive binding experiments of 6a/6b, 6a/6c, and 6a/6d with 1

MU211-213

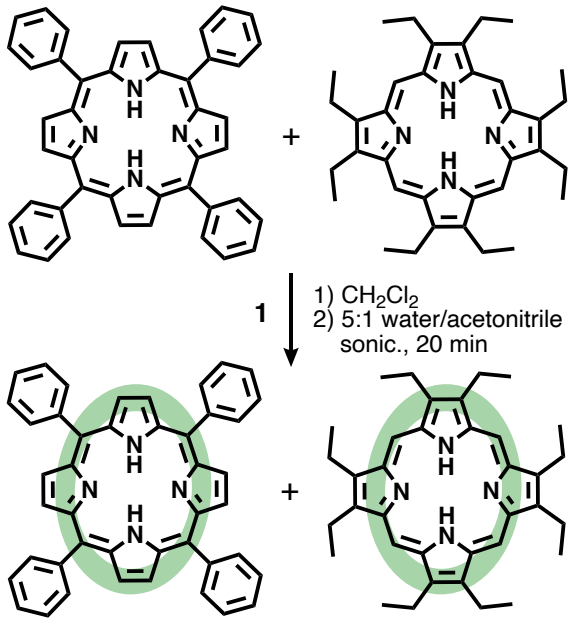

A CH_2Cl_2 solution (1.0 mM) of **6a** (0.14 mL, 0.14 μmol) and **6c** (0.14 mL, 0.14 μmol) were added to a glass tube including cage **1** (0.61 mg, 0.14 μmol). After evaporation of the solvent, the mixture was sonicated in 5:1 H_2O/CH_3CN (1.0 mL) for 20 min (40 kHz, 150 W). After the removal of excess **6a** and **6c** by centrifugation and filtration, the solution was lyophilized to analyze the ratio of bound **6a** and **6c**. The

resultant solid was dissolved in $CHCl_3$ and then free **1** was removed from the solution by silica gel filtration. The 5:1 ratio of **6a** and **6c** bound by **1** was estimated by ^1H NMR analysis. The competitive binding experiments of **6a** and **6b** as well as **6a** and **6d** with **1** were examined under the same conditions.

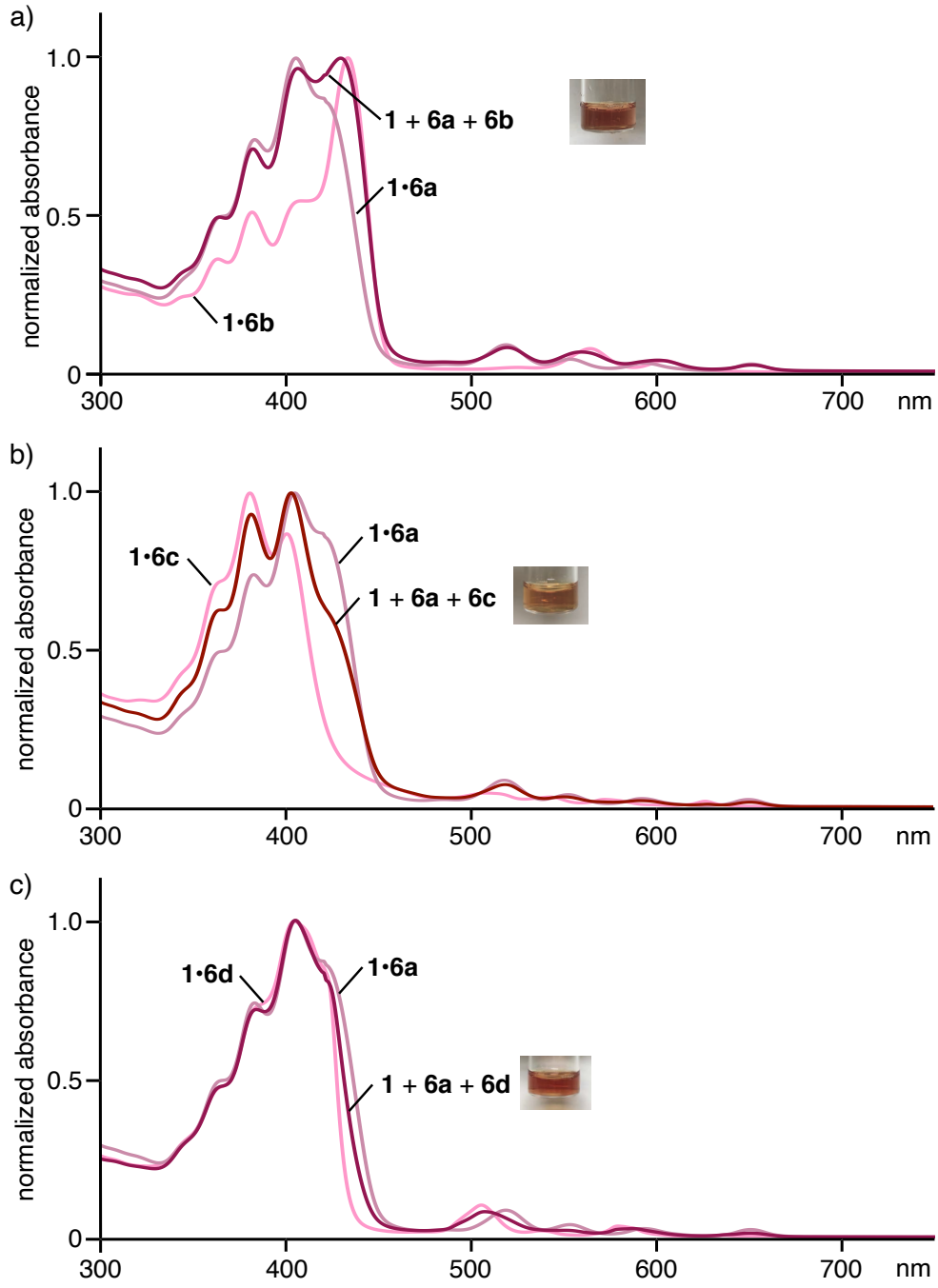

Figure S44. UV-visible spectra (r.t., 5:1 H_2O/CH_3CN, 0.14 mM based on **1**) of products after the competitive binding experiments of a) **6a** and **6b** with **1**, b) **6a** and **6c** with **1**, and c) **6a** and **6d** with **1**.

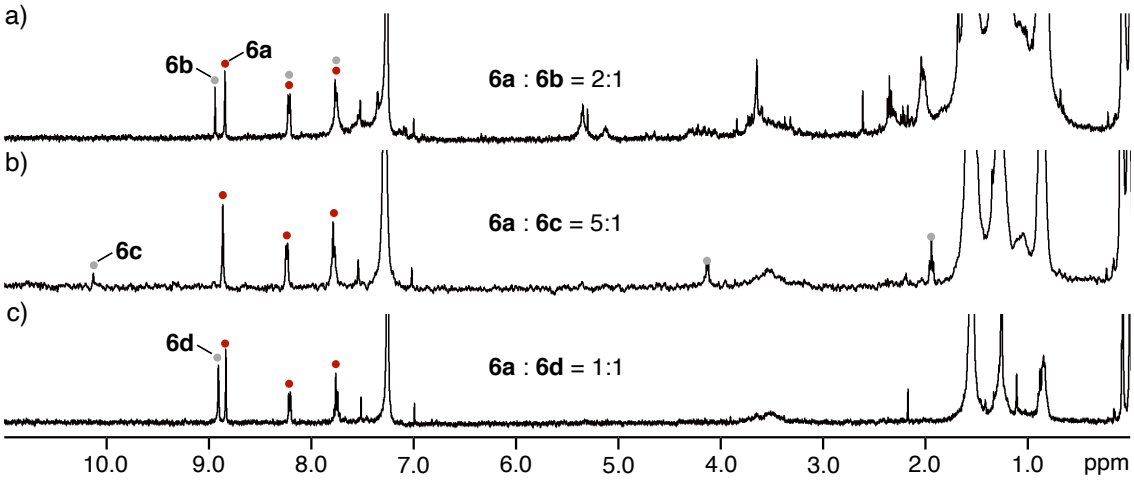

Figure S45. ^{1}H NMR spectra (400 MHz, $CDCl_3$, r.t.) of products after the competitive binding experiments of a) **6a** and **6b** with **1**, b) **6a** and **6c** with **1**, and c) **6a** and **6d** with **1**.